HHS Public Access

Author manuscript

Dev Cell. Author manuscript; available in PMC 2021 December 07.

Published in final edited form as:

Dev Cell. 2020 December 07; 55(5): 603–616.e5. doi:10.1016/j.devcel.2020.10.019.

Regulation of ARGONAUTE10 Expression Enables Temporal and Spatial Precision in Axillary Meristem Initiation in *Arabidopsis*

Cui Zhang[1,2,3,5,6], **Lusheng Fan**[3], **Brandon H. Le**[3], **Peiyi Ye**[4], **Beixin Mo**[1,2], **Xuemei Chen**[3,7,*]

[1]Guangdong Provincial Key Laboratory for Plant Epigenetics, College of Life Sciences and Oceanography, Shenzhen University, Shenzhen 518060, China

[2]Key Laboratory of Optoelectronic Devices and Systems of Ministry of Education and, Guangdong Province College of Optoelectronic Engineering, Shenzhen University, Shenzhen, Province 518060, China

[3]Department of Botany and Plant Sciences, Institute of Integrative Genome Biology, University of California, Riverside, CA 92521, USA

[4]State Key Laboratory of Plant Genomics, Institute of Genetics and Developmental Biology, Chinese Academy of Sciences, and National Center for Plant Gene Research, Beijing 100101, China

[5]Present address: Key Laboratory of Plant Molecular Physiology, CAS Center for Excellence in Molecular Plant Sciences, Institute of Botany, Chinese Academy of Sciences, Beijing 100093, China

[6]Present address: University of Chinese Academy of Sciences, Beijing 100049, China

[7]Lead Contact

SUMMARY

Axillary meristems (AMs) give rise to lateral shoots and are critical to plant architecture. Understanding how developmental cues and environmental signals impact AM development will enable the improvement of plant architecture in agriculture. Here, we show that ARGONAUTE10 (AGO10), which sequesters miR165/166, promotes AM development through the miR165/166 target gene *REVOLUTA*. We reveal that *AGO10* expression is precisely controlled temporally and spatially by auxin, brassinosteroids, and light to result in AM initiation only in the axils of leaves at a certain age. *AUXIN RESPONSE FACTOR 5* activates while *BRASSINAZOLE-RESISTANT 1*, and *PHYTOCHROME-INTERACTING FACTOR 4* repress *AGO10* transcription directly. In axils of young leaves, *BZR1* and *PIF4* repress *AGO10* expression to prevent AM initiation. In axils of older leaves, *ARF5* upregulates *AGO10* expression to promote AM initiation. Our results

*Correspondence: xuemei.chen@ucr.edu.

AUTHOR CONTRIBUTIONS

Conceptualization and Methodology, C.Z. and X.C.; Investigation, C.Z., P.Y., B.L., L.F., and X.C.; Formal Analysis, C.Z., L.F., P.Y., and X.C.; Supervision, B.M. and X.C.; Writing – Original Draft, C.Z. and X.C.; Writing – Review & Editing, all authors.

DECLARATION OF INTERESTS

The authors declare no competing interests.

SUPPLEMENTAL INFORMATION

Supplemental Information can be found online at https://doi.org/10.1016/j.devcel.2020.10.019.

uncover the spatiotemporal control of AM development through the cooperation of hormones and light converging on a regulator of microRNA.

In Brief

Axillary meristems (AMs) give rise to lateral shoots. Understanding how AM development is regulated will enable the improvement of plant architecture. Zhang et al. find that *ARGONAUTE10* expression is controlled by auxin, brassinosteroids, and light to result in AM initiation in a spatiotemporally precise manner.

Graphical Abstract

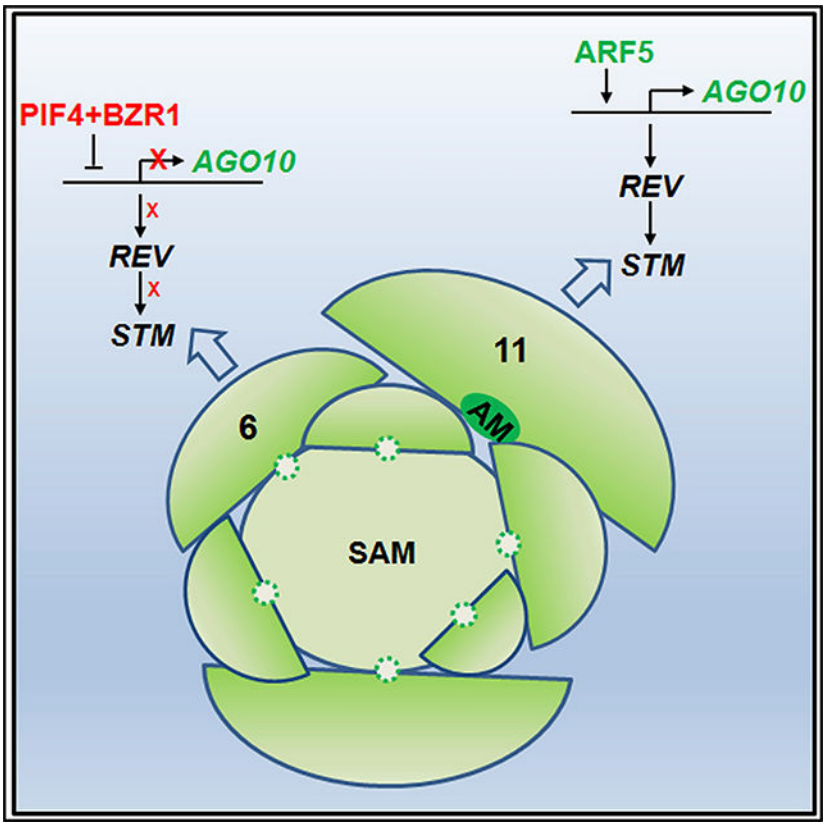

INTRODUCTION

Lateral shoots are key structures that contribute to plants' above-ground morphology and yield. The development of lateral shoots entails stem cell maintenance, axillary meristem (AM) initiation, AM differentiation, and bud outgrowth. AMs are formed from a small number of stem cells with meristematic competence located in leaf axils (Burian et al., 2016). As reflected by the expression of the meristematic marker *SHOOT MERISTEMLESS* (*STM*) (Barton and Poethig, 1993), the stem cells are dynamically regulated in leaf axils at different stages. The stem cells are maintained with low *STM* expression in young leaf axils (< P_{10}) and are activated to form the AM with high *STM* expression in older leaf axils around P_{11} (Shi et al., 2016). As AMs initiate from the

boundary region between the stem and a leaf, genes that specify boundary identity impact AM formation. These include *CUP-SHAPED COTYLEDON* (*CUC*) (Hibara et al., 2006; Raman et al., 2008), *LATERAL SUPPRESSOR* (*LAS*) (Greb et al., 2003), *REGULATOR OF AXIL-LARY MERISTEMS* (Müller et al., 2006), and *LATERAL ORGAN BOUNDARY* (*LOB*) (Shuai et al., 2002). These genes are expressed throughout the boundary region at the base of young leaves; thus, their expression is spatially broader than the point where AM initiates and temporally much earlier than AM initiation. However, *REVOLUTA* (*REV*) expression is coincidental with AM initiation. *REV* belongs to the HD-ZIPIII family that is targeted by miR165/166 and is the only member in this family that activates stem cells toward AM initiation (Otsuga et al., 2001; Talbert et al., 1995b). Loss of function of *REV* leads to the absence of AMs (Talbert et al., 1995a). Although *REV* is expressed throughout the adaxial domain of leaf primordia, *REV* expression is low in young leaf axils and increases in older leaf axils at the time and place of AM initiation. *REV* was found to promote AM initiation by activating *STM* expression (Shi et al., 2016). Thus, uncovering the mechanisms that contribute to the specific patterns of *REV* expression is probably key to understanding how AMs are initiated in a spatiotemporally specific manner.

The expression of the HD-ZIPIII family genes including *REV* is repressed at the posttranscriptional level by miR165/166 (Bao et al., 2004; Juarez et al., 2004; Mallory et al., 2004). The *MIR165/166* genes are expressed on the abaxial epidermis of leaves and in the endodermis of roots, but the mature miRNA is found in a broader domain and silences HD-ZIPIII genes to specify leaf polarity and root vasculature development (Carlsbecker et al., 2010; Chitwood et al., 2009; Tatematsu et al., 2015). While miR165/166 acts through ARGONAUTE1 (AGO1), AGO10 preferentially binds miR165/166 to sequester the miRNA from AGO1 (Zhu et al., 2011) and to lead to the degradation of the miRNA (Yu et al., 2017), thus, promoting the expression of HD-ZIPIII genes (Ji et al., 2011; Liu et al., 2009). Loss of function in *AGO10* results in stem cell termination in the shoot apical meristem (SAM) due to ectopic activity of miR165/166 (Liu et al., 2009; Lynn et al., 1999; Zhu et al., 2011). Stem cells in AMs share common characteristics with those in the SAM. In fact, *ago10* mutants have fewer lateral branches (Lynn et al., 1999), suggesting that *AGO10* is required for AM development.

It is likely that common endogenous and external signals impact the development of the SAM and AMs. The plant hormone auxin plays a major role in developmental patterning including meristem specification and organization. Auxin controls stem cell homeostasis partly through *AUXIN RESPONSE FACTOR 5* (*ARF5*, also named *MONOPTEROS*, *MP*) in the SAM (Luo et al., 2018). Auxin is also necessary for cambium meristem organization in vascular development; ectopic expression of *ARF5* induces ectopic cambium meristem formation (Miyashima et al., 2019; Smetana et al., 2019). Stem cells form in leaf axils at a central position that exhibits an auxin minimum, and elevation of auxin levels in leaf axils through the expression of the Agrobacterial *iaaM* auxin biosynthesis gene inhibits the formation of AM stem cells, suggesting that auxin plays a negative role in AM stem cell maintenance (Wang et al., 2014a, 2014b). Brassinosteroids (BRs) are another class of plant hormones; *BRASSINAZOLE-RESISTANT 1* (*BZR1*) encodes a major transcription factor acting downstream of the BR signaling pathway (He et al., 2005; Wang et al., 2002). The fact that *BZR1* represses *CUC3* transcription implies a negative role of BR in boundary

formation (Gendron et al., 2012). But it is unknown whether BR affects AM initiation. Light regulates multiple physiological processes throughout plant life. Although light intensity, quality, and photoperiod influence bud outgrowth (Leduc et al., 2014), the molecular basis is poorly understood, and it is unknown whether light affects AM initiation. Photomorphogenesis is regulated partly through phytochromes and the antagonizing PIF transcription factors. Phytochrome B (PhyB) senses red light and inhibits PIF4 activity by ubiquitin-mediated proteasome degradation (Huq and Quail, 2002). Intriguingly, *phyB* mutants display fewer lateral buds (Finlayson et al., 2010; Leduc et al., 2014), which implicates a role of light signal perception and transduction in AM initiation.

In this study, we showed that *ago10* loss-of-function mutants exhibit defects in AM initiation and that *AGO10* promotes AM initiation through the activation of *REV*. *AGO10* expression exhibits temporal and spatial precision that matches the spatiotemporal patterns of AM initiation: *AGO10* is expressed at the center of the stem/leaf boundary, where AMs initiate; its expression starts at the axils of leaves at the P_{11} stage, a stage when AMs initiate. We demonstrated that the spatiotemporal patterns of *AGO10* expression are achieved by co-regulation by auxin, BR, and light signals through *ARF5*, *BZR1*, and *PIF4*, respectively. While *PIF4* is expressed ubiquitously in leaves, the adaxially expressed *BZR1* acts together with *PIF4* to directly repress *AGO10* expression in young leaf axils. In contrast, *ARF5*, expressed predominantly on the adaxial side of leaves and older leaf axils, directly activates *AGO10* expression in initiating AMs. These hormonal and environmental signals cooperate to regulate *AGO10* expression to ensure AM initiation at a distance from the SAM.

RESULTS

ago10 Mutants Exhibit AM Defects

Mutants in *AGO10* in the Landsberg (Ler) background exhibit a pin-like SAM indicative of stem cell defects (Mcconnell and Barton, 1995). Besides the shoot apex, *ago10* mutants show reduced lateral buds in axils of cauline leaves (Lynn et al., 1999). Since AMs and SAM share common features, we investigated whether *AGO10* influences AM formation. We first observed AM morphology of the strong *ago10* mutant *pnh-2* (Mcconnell and Barton, 1995) using scanning electron microscopy. While wild-type plants had obvious lateral buds in axils of mature rosette leaves, *pnh-2* plants tended to lack lateral buds (Figures 1A and 1B). To quantify the phenotype, we counted the number of AMs in each leaf axil. In *pnh-2* and *ago10–13* (Ji et al., 2011) plants (both in the Ler background), a clear reduction in AM number was found, with early leaves showing more deficiency than later leaves in AM formation in their axils (Figure 1C). The position of AM deficiency along the shoot varied in different *ago10* alleles, a phenotype that resembled that of *rax* mutants, but the underlying mechanisms are unknown (Müller et al., 2006). In contrast to the loss-of-function mutants, plants that overexpress *AGO10* occasionally had more than one AM per leaf axil, particularly for late-developing rosette leaves and some cauline leaves (Figure 1C). We further examined AMs through tissue sections. While wild-type plants showed a population of meristematic cells with dark staining in leaf axils (Figure S1A), *pnh-2* plants had fewer cells with dark staining in leaf axils (Figure S1B). Wild-type plants had an obvious, dome-shaped AM in the axil of the fifteenth primordium (P_{15}) (Figure S1C), *pnh-2*

plants did not show an AM bulge at the same stage (Figure S1D). These results suggested that *AGO10* is required for AM initiation in *Arabidopsis*.

AM initiation is regulated temporally and spatially: an AM is initiated in the center of the axil of the P_{11} leaf. To determine whether *AGO10* is expressed at the time and position of AM initiation, we observed YFP-AGO10 signals in *pZLL::YFP-ZLL zll-1* plants in which the *zll-1* (an *ago10* allele) mutant phenotype was fully rescued by *YFP-ZLL* (*ZLL* is *AGO10*) (Tucker et al., 2008). YFP-AGO10 signals were predominantly in the SAM, vasculature, and adaxial side of leaf primordia (Figures 2A and 2B). In leaf axils, YFP-AGO10 was specifically present in developing AMs located at the center of the leaf axil but not in the surrounding boundary region (Figures 2C and 2D). Temporally, YFP-AGO10 was only present at the axils of P_{11} leaves and beyond. The temporal and spatial patterns of *AGO10* expression coincided perfectly with those of AM initiation.

AGO10 Promotes AM Development through Activating *REV* and *STM* Expression

Previous reports showed that the expression of the HD-ZIPIII family genes and the meristem marker gene *STM* is reduced in the SAM of *ago10* mutants (Lynn et al., 1999). In the HD-ZIPIII family, *REV* plays a specific role in AM development (Talbert et al., 1995a) through activating *STM* expression (Shi et al., 2016). Thus, we examined *REV* and *STM* expression using reverse-transcription quantitative PCR (qRT-PCR). The results showed that *REV* and *STM* expression levels decreased in the *pnh-2* mutant and increased in the *AGO10* overexpression line *p35S::AGO10* as compared with wild type (Figures 3A and 3B). To examine REV and STM expression patterns in planta, we crossed the marker lines *pREV::REV-Venus* and *pSTM::STM-Venus* (Heisler et al., 2005) to the *pnh-2* mutant. REV-Venus signals were present in AMs of wild-type plants (Figures 3C and 3E) but nearly undetectable in AMs of the *pnh-2* mutant (Figures 3D and 3F). STM-Venus signals were present at the boundary between the SAM and young leaf primordia in wild-type plants (Figure 3G, signals near the asterisk). STM-Venus signals were also present at the boundary between the SAM and young leaf primordia in *pnh-2*, albeit at lower levels (Figure 3H inset). In AMs in axils of P11 and older leaves, STM-Venus signals were much weaker in *pnh-2* compared with wild type (Figures 3G–3J). Thus, *AGO10* seemed to promote the expression of *REV* and *STM*. The *rev* strong allele *rev-6* and the *stm* weak allele *stm-bum1* showed an AM deficiency phenotype stronger than that of *pnh-2* (Figure S1E), suggesting that *AGO10*-independent mechanisms also promote *REV* and *STM* expression. To analyze the relationship between *AGO10* and *STM* genetically, we introduced an inducible *STM* transgene, *p35S::STM-GR* (Heisler et al., 2005), into *pnh-2* through crosses. The STM-GR fusion protein is expected to translocate into the nucleus to function upon dexamethasone (Dex) treatment. Dex, but not mock, treatment led to AM formation in *p35S::STM-GR pnh-2* (Figures S1F–S1H). These results indicated that *STM* functions downstream of *AGO10*. Sequestration of miR165/166 by target mimicry (*p35S::STTM165/166*) (Yan et al., 2012) rescued the AM defects of *pnh-2* (Figures S1E and S1I). Taken together, *AGO10* promotes AM development through sequestration of miR165/166, leading to the activation of *REV* and *STM* expression.

Auxin, BR, and Light Signaling Pathways Regulate AM Development

AGO10 displays highly specific patterns of expression that coincide with the timing and position of AM development. To search for the potential upstream signals that specify *AGO10* expression, we analyzed the promoter of *AGO10*. Specific motifs including auxin response element (ARE) (Ulmasov et al., 1995), brassinosteroid response element (BRRE) (He et al., 2005), and light response elements (E-box and G-box, a variant of E-box with more affinity for PIF4) (Huq and Quail, 2002) were found within ~5,000 base pairs upstream of the translation start site of *AGO10* (Figure S2A). To test whether *AGO10* expression responded to the hormonal and light signals, we treated seedlings with various hormones and with light and measured *AGO10* transcript levels using boundary-enriched shoot apices (apices with leaves removed). The qRT-PCR results showed that *AGO10* expression was significantly upregulated by auxin treatment and by light, and downregulated by BR, but was only slightly affected by other hormones/chemical such as ABA, JA, and ACC (precursor to ethylene) (Figure S2B). Although there are cytokinin response elements in the *AGO10* promoter, cytokinin treatment did not result in as large a change in *AGO10* expression compared with auxin, BR, and light (Figures S2B and S2D). Interestingly, many more cytokinin response elements are present in the *AGO1* promoter and *AGO1* expression responded strongly to cytokinin (Figure S2C). In contrast to *AGO10*, *AGO1* expression was more ubiquitous in leaves and AMs (Figures S2E–S2I). Taken together, auxin, BR, and light signals may contribute to the regulation of *AGO10* expression.

To analyze whether and how the three signals control AM development, we observed the AM phenotype of mutants in genes in the corresponding signal transduction pathways. An auxin pathway mutant, *pinoid-8*, which is disrupted in polar auxin transport, and two auxin-resistant mutants, *axr1–3* and *axr1–12*, showed a decrease in AM number (Figure S3A), indicating a positive role of auxin in AM development. As auxin functions through *ARF* genes, we observed the AM phenotype in various *arf* mutants. None of the *arf2*, *arf3*, *arf4*, and *arf16* mutants showed an obvious AM defect, whereas the *arf10* mutant showed AM deficiency in early rosette leaves (Figure S3A) (Wang et al., 2005). Because *arf5* mutants exhibit severe SAM defects (Luo et al., 2018), we analyzed the AM phenotype of *arf5*. Strong *arf5* (also known as *mp*) mutants are seedling lethal (Berleth and Jurgens, 1993). *mps319* (*arf5–2*) is a weak allele—the plants undergo vegetative and reproductive development but fertility is low (Figures S4A and S4B) (Schlereth et al., 2010). We partially rescued the strong phenotype of *mp* with *pAR-F5*::*ARF5-GFP* and obtained a transgenic line *pARF5::ARF5-GFP mp* that resembled *mps319* in fertility. In this partially rescued line, *ARF5* expression level was lower than that in wild type (Figure S4C). In both *mps319* and *pARF5::ARF5-GFP mp*, the number of AMs was significantly lower than wild type (Figures S4C–S4H). Thus, proper AM initiation requires polar auxin transport and *ARF5*.

In the BR pathway, the biosynthesis mutant *det2* (Chory et al., 1991; Li et al., 1997) or the BR-insensitive mutant *bri1–5* (Noguchi et al., 1999) did not show any defects in AM number (Figure S3B). BES1 and BZR1 are two homologous transcription factors functioning redundantly in the BR signaling pathway (Li et al., 2018). *BES1* RNAi lines with low levels of *BES1* and *BZR1* expression (Yin et al., 2005) did not show any AM defects (Figure S3B). The dominant mutant *bzr1–1D* with increased BZR1 activity showed a significant reduction

in AM number in early rosette leaves (Figure S3B). BZR1 is known to repress *CUC3* transcription in the SAM-leaf boundary (Gendron et al., 2012). This, together with the AM defects in *bzr1–1D* plants, suggests that BR plays a negative role in AM development.

The red light receptor mutants *phyB-5* and *phyB-9*, in which PIF activity is increased (Huq and Quail, 2002), showed a reduction in AM number in early rosette leaves (Figure S3C). Mutants of the *PIFs* did not show AM defects: either *pif1, pif3*, *pif5* single mutants or the *pif1/3/4/5* quadruple mutant (*pifQ*) (Leivar et al., 2008) were normal in AM development. In contrast, the *PIF4* overexpression (*PIF4 OX*) line *pPIF4::PIF4-Citrine-HA* (Yamashino et al., 2013) showed a reduction in AM number in early rosette leaves (Figure S3C). This implied that light positively regulates AM development by suppressing *PIF4*.

ARF5, *BZR1*, and *PIF4* Regulate *AGO10* Expression in AMs

We first examined the expression patterns of *ARF5*, *BZR1*, and *PIF4* using fluorescent protein fusions driven by the respective promoters. In *pARF5::ARF5-GFP* lines, ARF5-GFP signals were high on the adaxial side of young leaves but low in the SAM and in axils of young leaves, which is consistent with the low level of auxin in stem cells (Luo et al., 2018) (Figure 4A). ARF5-GFP signals were present on the adaxial side of older leaves, in the vasculature, and at developing AMs (Figure 4B). The expression patterns of *ARF5* were highly coincidental with those of *AGO10*. In *pBZR1*::*BZR1-CFP* and *pPIF4::PIF4-Citrine-HA* transgenic lines, BZR1-CFP and PIF4-Citrine-HA signals were present in the SAM, at the boundary of the SAM and young leaves, on the adaxial side of young leaves, and in AMs (Figures 4C–4F). The extensive overlap in expression patterns of *ARF5* and *AGO10* and the partial overlap in expression patterns of *BZR1* and *PIF4* with *AGO10* prompted us to test whether these genes contributed to the spatial and temporal regulation of *AGO10* in the AM.

To determine whether *ARF5*, *BZR1*, and *PIF4* regulate *AGO10* expression, we crossed the marker line *pZLL::YFP-ZLL* to *pAR-F5::ARF5-GFP mp*, *bzr1–1D*, and *phyB-9* plants, respectively. YFP-AGO10 signals in AMs were much lower in *pARF5::ARF5-GFP mp* (representing a weak *arf5* mutant) compared with wild type (Figures 4G and 4H), suggesting that *ARF5* promoted *AGO10* expression. Similar down regulation of YFP-AGO10 was observed in *bzr1–1D* and *phyB-9* plants (Figures 4G, 4I, and 4J), suggesting that BZR1 and PIF4 were both negative regulators of *AGO10* expression.

To analyze the effect of these transcription factors on the expression of the endogenous *AGO10* locus (rather than the transgene), we performed qRT-PCR with various genotypes. *AGO10* mRNA levels decreased in the *mps319* mutant and increased in the *ARF5* overexpression line *pARF5::ARF5-GFP* (*ARF5 OX*) when compared with wild type (Figure 4K), which suggested that *ARF5* activates *AGO10* expression. *AGO10* mRNA levels were decreased in the *bzr1–1D* mutant and increased in the *bri1–5* mutant (Figure 4K), indicating that *BZR1* represses *AGO10* expression. *AGO10* expression was increased in *pif4–2* and decreased in the *pPIF4::PIF4-Citrine-HA* overexpression line (Figure 4K), indicating that *PIF4* represses *AGO10* expression.

The above analyses implied that *AGO10* was downstream of the transcription factors in AM development. To confirm this genetically, we overexpressed *AGO10* in *pARF5::ARF5-GFP*

mp, bzr1–1D, pPIF4::PIF4-Citrine-HA, and *phyB-9* plants by crossing the *p35S::AGO10* transgene into these genetic backgrounds. The AM defects of plants of the above genotypes were rescued by *AGO10* overexpression (Figures S3D and S3E). In addition, the *pnh-2 pif4–2* double mutant showed similar AM defects as the *pnh-2* single mutant (compare Figures S3D with 1C). Taken together, the expression and genetic analyses indicated that *AGO10* functions downstream of *ARF5*, *BZR1*, and *PIF4* in AM development

ARF5, BZR1, and PIF4 Directly Regulate *AGO10* Expression

The *AGO10* promoter contained ARE, BRRE, and E-Box motifs known to be bound by ARFs, BZR1, and PIFs from the auxin, BR, and light signaling pathways, respectively (Figure 5A) (He et al., 2005; Huq and Quail, 2002; Ulmasov et al., 1995). This suggested that ARF5, BZR1, and PIF4 may bind the *AGO10* promoter to directly regulate *AGO10* expression. To determine whether these transcription factors bind to the *AGO10* promoter, we performed chromatin immunoprecipitation (ChIP)-qPCR. The results indicated that ARF5, BZR1, and PIF4 bound specific regions of the *AGO10* promoter that contained the corresponding motifs (Figures 5B–5D).

To analyze the effects of ARF5, BZR1, and PIF4 on *AGO10* promoter activity, we resorted to transient expression with leaf protoplasts. Each of the three transcription factors was introduced into protoplasts together with the firefly luciferase (*LUC*) reporter gene driven by the *AGO10* promoter (Figure 6A). A *p35S::REN* transgene encoding Renila luciferase in the same construct was used as an internal control for transfection efficiency. ARF5 dramatically increased Luc activity as compared with the empty vector, indicating that ARF5 activated *LUC* expression through the *AGO10* promoter (Figure 6B). Both BZR1 and PIF4 reduced Luc activity, indicative of their repressive effects on the *AGO10* promoter (Figures 6C and 6D). To determine whether the transcription factors acted through the putative elements in the *AGO10* promoter, we deleted the elements individually or together (Figure 6E) and assayed *LUC* expression in the presence of the transcription factors. Deletion of the two ARE motifs (Δ12) abolished the activation of *LUC* expression by ARF5; deletion of the first ARE motif (Δ1), but not that of the second ARF motif (Δ2), greatly decreased Luc activity (Figure 6F). Thus, ARF5 acted mainly through the first ARE to promote *AGO10* expression. Deletion of the BRRE (Δ3) abolished the repressive effects of BZR1 on the *AGO10* promoter, indicating that BZR1 acted through the BRRE motif to repress *AGO10* expression (Figure 6G, compare *pAGO10* and *Δ3* in the presence of BZR1-GFP). Deletion of the G-box (Δ4) abolished the repression of *pAGO10::LUC* by PIF4-GFP, indicating a negative role of the G-box in transcriptional repression of *AGO10* mediated by PIF4 (Figure 6H, compare *pAGO10* and *Δ4* in the presence of PIF4-GFP). These results indicate that ARF5, BZR1, and PIF4 directly regulate *AGO10* transcription through binding to the core responsive elements.

To test the potential role of the motifs in specifying *AGO10* expression *in planta*, we used *pAGO10* with deletions in the binding motifs to drive *GFPer* expression. While the native *AGO10* promoter resulted in GFP signals in the SAM and on the adaxial side of young leaves (Figure S5A), the transgenes containing deletions of the BR and light response elements (*pAGO10Δ34::GFP*) showed an expanded *GFP* expression zone, with GFP signals

being present throughout the leaves (Figure S5B). Thus, BZR1 and/or PIF4 were responsible for repressing *AGO10* expression on the abaxial side of leaves. The ARE-deleted *AGO10* promoter conferred lower GFP signals (Figure S5C), suggesting that auxin promotes *AGO10* expression quantitatively. In conclusion, the motifs located in the *AGO10* promoter are important for the strengths or the spatial patterns of *AGO10* expression.

We next examined the relevance of the transcription factorbinding sites in the *AGO10* promoter during AM formation. We generated *pAGO10D1*, a line with a deletion of the ARF5-binding site in the *AGO10* promoter by Crispr-Cas9. Deletion of the ARF5-binding site in the *AGO10* promoter (Figure S4I) caused AM deficiency similar to *pARF5::ARF5-GFP mp* (mimicking a weak *arf5* allele) and *mps319* (a weak *arf5* allele) (Figures 6I and S4H), validating the importance of the ARF5-binding site in AM formation. We transformed *bzr1–1D* with *AGO10* driven by the BZR1-binding site deleted promoter (*pAGO10Δ3*) and the AM defects of *bzr1–1D* were rescued in the transgenic plants (Figure 6I), validating the importance of the BZR1-binding site in inhibition of AM initiation. We transformed *PIF4 OX* with *AGO10* driven by the PIF4-binding site deleted promoter (*pAGO10Δ4*), and the AM defects of *PIF4 OX* were rescued in the transgenic plants (Figure 6I), indicating that *PIF4* represses *AGO10* expression through this binding site to inhibit AM initiation.

ARF5, BZR1, and PIF4 Co-regulate *AGO10* Transcription Temporally and Spatially during AM Development

To analyze the combinatorial effects of ARF5, BZR1, and PIF4 on *AGO10* expression, we performed protoplast transient expression assays using different combinations of these three transcription factors together with *LUC* driven by the native *AGO10* promoter. ARF5 activated *pAGO10::LUC* expression in protoplasts (Figures 6B and S5D). However, when protoplasts were transfected with both *ARF5* and *BZR1*, Luc activity decreased significantly compared with *ARF5* alone (Figure S5D). Similarly, co-transfection of *PIF4* and *ARF5* resulted in lower Luc activity when compared with *ARF5* alone (Figure S5D). Thus, BZR1 and PIF4 played antagonistic roles to ARF5 and attenuated its function in activating *AGO10* transcription.

To investigate the functions of the three transcription factors *in vivo*, we first examined the temporal and spatial patterns of *ARF5*, *BZR1*, and *PIF4* expression using fluorescent protein fusions driven by the respective promoters. ARF5-GFP was found on the adaxial side of young leaves (<P_6), the middle zone of P_6–P_{10} and eventually in the vasculature and on the adaxial side of older leaves just before AM initiation (P_{11}, Figures 7A and 7B). The expression patterns of *ARF5* were the same as those of *AGO10* (Figure 2). PIF4-Citrine persisted on the adaxial side of all leaves and was present throughout the stages of AM development (Figures 7C, 7D, and 4F). In contrast, BZR1-CFP signals were on the adaxial side of young leaves (<P_{10}), disappeared in leaves when AMs will initiate (P_{10}–P_{11}, Figure 7F), and resumed in established AMs (Figure 4D). Interestingly, BZR1 expression levels showed a high-to-low gradient from the adaxial side to the abaxial side, with more nuclear localization on the adaxial side and more cytoplasmic localization on the abaxial side in young leaves (Figure 7E). In contrast, the expression patterns were altered in *pBZR1::BZR1m-CFP* transgenic lines, in which a BZR1 phosphorylation site was mutated

leading to constitutive activity of BZR1 (Figure 7G) (Wang et al., 2002). BZR1m lacked the gradient in young leaves (P_8, Figure 7H) and showed persistent expression in older leaves (P_{11}, Figure 7H, compare with Figure 7F). These results indicate that BZR1 phosphorylation is necessary for its specific patterns of accumulation. In addition, *pBZR1::BZR1m-CFP* plants showed similar AM defects as the *bzr1–1D* mutant (Figures S5E and S5F) and more severe AM defects than *pBZR1::BZR1-CFP* plants (Figure S5F), implying a role of BZR1 phosphorylation in AM development. From the temporal and spatial expression patterns, we propose that *BZR1* and *PIF4* repress *AGO10* transcription in young leaves while *ARF5* activates *AGO10* transcription in older leaves, which explains the temporal activation of *AGO10* expression and AM initiation in older leaf axils.

We next examined the interactions among *ARF5,BZR1*, and *PIF4* genetically. The *ARF5* overexpression line *pARF5::ARF5-GFP* showed AMs almost in every leaf axil similar to wild type (Figure S5E). The *bzr1–1D* dominant mutant showed an absence of AMs in about the first eight rosette leaves. The *pARF5::ARF5-GFP bzr1–1D* plants showed increased AM number in early rosette leaves when compared with *bzr1–1D* plants, which indicates that *ARF5* antagonizes *BZR1* in AM development (Figure S5E). Plants harboring weak alleles of *ARF5*, *mps319*, and *pARF5::ARF5-GFP mp*, showed a reduction in AM number in about the first fifteen rosette leaves (Figure S4H). The loss-of-function mutant *pif4–2* had AMs in almost every leaf axil similar to wild type (Figure S5E). The *pif4–2 mps319* plants displayed an increase in AM number in early rosette leaves (Figure S5E) compared with the respective *ARF5* knockdown alleles (Figure S4H), which indicates antagonism between *ARF5* and *PIF4* in AM development. On the other hand, *bzr1–1D* and *phyB-9* both showed AM deficiency in early rosette leaves (Figures S3B and S3C) and the double mutant showed enhanced AM deficiency (Figure S5E), suggesting that *BZR1* and *PIF4* repress AM development redundantly.

Duo Functions of Auxin in AM Development

Previous studies showed that auxin inhibits the maintenance of stem cells that would later give rise to AMs (Wang et al., 2014a, 2014b). Our studies suggest a positive role of auxin in AM initiation and development through *ARF5*. To define the stage at which the positive role of auxin is essential, we first examined the distribution of auxin during AM development using the auxin response reporter *DR5* and the sensor reporter *DII-Venus* (Vernoux et al., 2011). *pDR5::GFP* signals were detected in early-stage AMs in leaf axils (P_{11}, Figure S6A) and then in specific zones of late-stage AMs (P_{16}, Figure S6B). In contrast, *p35S::DII-Venus* signals were low in both early- and late-stage AMs (P_{12} and P_{14}, Figure S6D). This confirms that auxin is present in newly initiated AMs as in the SAM (Figure S6C). Next, we further examined *ARF5* function during AM development using the *mpΔ* allele with constitutively active *ARF5* (Krogan et al., 2012). The AMs in the *mpΔ* mutant appeared larger (Figure S6F) than those in the axils of the same-staged leaves in wild type (P_{12}, Figure S6E), suggesting that AMs were developmentally advanced due to constitutive activity of *ARF5* in *mpΔ*. This phenotype is consistent with our findings that *ARF5* promotes AM initiation. Deletion of the ARF5-binding site in the *AGO10* promoter (*pAGO10D1*) rescued the AM defects of *mpΔ* (Figure S6G), which confirms that *ARF5* regulates AM development through *AGO10*. Next, we sought to distinguish the early, stem cell maintenance stage and

the later AM initiation stage in the weak *arf5* mutant *mps319* using the *pSTM::STM-Venus* marker. STM-Venus signals were present in axils of young leaves of *mps319* plants (Figures S6H and S6I) as in *pnh-2* (Figure 3H), suggesting that stem cells were maintained in axils of young leaves of both *mps319* and *pnh-2* before AM initiation. But STM-Venus signals decreased dramatically in axils of leaves when AM initiates in *mps319* (Figure S6I) and *pnh-2* (Figure 3H) as well as *rev-6* (Shi et al., 2016). Thus, like *REV*, *ARF5* and *AGO10* are required to activate *STM* expression at the stage of AM initiation. Based on the above results, we propose that auxin, while playing a negative role in stem cell maintenance, promotes the activation of the stem cells for AM initiation at a later stage.

The antagonistic roles of *ARF5* and *BZR1* in *AGO10* transcription implies that auxin and BR are competing forces that maintain a balance during AM development. We explored *in vitro* treatment with the hormones (IAA, active form of auxin; or BL, active form of BR) at both the shoot apex and leaf axils. In *pAGO10::YFP-AGO10* plants with both endogenous *AGO10* and transgenic *AGO10*, a moderate phenotype was present including occasionally two AMs in one leaf axil (Figure S6J). BR treatment suppressed the two-AMs-per-leaf-axil phenotype (Figure S6J), whereas auxin treatment enhanced this phenotype (Figure S6J). The phenotype induced by auxin treatment was similar to that induced by *AGO10* overexpression (Figure 1C). Consistently, *AGO10* expression was increased by auxin and reduced by BR (Figure S6K). Interestingly, when auxin and BR were applied together to leaf axils, the AM phenotype caused by each single hormone treatment was attenuated (Figure S6K). In addition, *AGO10* expression did not show significant changes under the combined hormone treatment in comparison with mock treatment (Figure S6K). Taken together, these results suggest that a balance between auxin and BR is vital for AM initiation.

DISCUSSION

AGO10 Function in AM Development

AM development can be divided into four stages: stem cell maintenance, AM initiation (activation), lateral organ differentiation, and bud outgrowth/dormancy (Figure S7A). In this study, we investigated the role of *AGO10* in AM initiation. We found that *AGO10* promotes AM initiation through activating *REV* and *STM* expression. *AGO10* exhibits spatially and temporally specific expression that coincides with AM initiation. *ARF5*, *BZR1*, and *PIF4* specify *AGO10* expression patterns by direct transcriptional regulation. Our results demonstrate the function of auxin, BR, and light in the early development of AMs.

An AM initiates from a group of meristematic cells located at the base of the adaxial side of a leaf. The division and differentiation of these meristematic cells are strictly regulated temporally and spatially. Strong and localized *STM* expression marks the initiation of the AM and commences just before an AM structure forms (P_{11}, Figure 7I). *REV* promotes AM initiation through activating *STM* in the early stage of AM development (P_{11}, Figure 7I). *AGO10* shows the same expression patterns as *REV*: both genes are first expressed on the adaxial side of young leaves (P_3), then in the middle zone where the vasculature begins to form (P_6), and eventually in the vasculature and the leaf axil just before AMs initiate (P_{11}, Figure 7I). *AGO1* is expressed more ubiquitously than *AGO10*. In young leaves (P_3, Figure S2G), *AGO1* is expressed throughout the leaf. In older leaves (P_6, Figure S2H), *AGO1* is

expressed strongly in the middle zone and weakly on the adaxial side. In mature leaves before AM initiation (P_{11}, Figure S2H), *AGO1* exhibits a low level of expression in the vasculature and at the leaf axil (Figure 7I). The specific expression of *AGO10* in AMs probably suppresses the activity of miR165/166-AGO1 to enable the temporally and spatially precise activation of *REV* expression and AM initiation.

Crosstalk among Auxin, BR, and Light Converges on *AGO10*

ARF5 exhibits the same expression patterns as *AGO10*: on the adaxial side of P_3, in the middle zone of P_6 and in the vasculature and at the axil of P_{11} (Figure 7I). *BZR1* is expressed mainly on the adaxial side of young leaves (P_3–P_6) and in the vasculature of mature leaves (P_{11}, Figure 7I). *PIF4* expression persists on the adaxial side of young leaves (P_3–P_6) and in AMs and the vasculature in older leaves (P_{11}, Figure 7I). In newly emerged leaves (before P_3), adaxially expressed *REV*, *AGO10*, and *ARF5* act together with abaxially expressed *ARF2*, *3*, and *4* to specify polarity (Chitwood et al., 2009; Guan et al., 2017; Heisler et al., 2005; Liu et al., 2009). After adaxial-abaxial polarity specification, the vasculature is formed in the middle zone of older leaves (such as P_6). *REV*, *AGO10* and *ARF5* are all expressed in the middle zone and play a role in vasculature development (Dinneny and Yanofsky, 2004; Smetana et al., 2019; Tucker et al., 2008). In this work, we found that *BZR1*, *PIF4*, and *AGO1* are also expressed here, but their functions in this region are currently unknown. At this stage, AMs are not yet formed. The negative regulators *BZR1* and *PIF4* are highly expressed in the axils of young leaves and repress *AGO10* expression, thus, inhibiting AM initiation (Figures 7I and S7B). After the formation of the vasculature, the leaves begin to initiate AMs in their axils (about P_{11}). At this stage, *AGO10* expression is increased by the activator *ARF5*, meanwhile the expression of the repressor *BZR1* is decreased (Figure 7I). The increased *AGO10* expression in turn leads to the activation of the downstream genes *REV* and *STM*, resulting in AM initiation (Figure S7B).

The spatiotemporal expression patterns of *AGO10* are likely specified by auxin, BR, and light signals. Auxin, which acts through ARFs, is a major hormone that modulates the development of the SAM. Previous research showed that auxin depletion is a prerequisite for establishing the stem cell niche that is responsible for AM formation at leaf axils (Wang et al., 2014a, 2014b). However, in this study, we found that auxin promotes the initiation of AMs through *ARF5*. Reduction-of-function mutants in *ARF5* show a reduction in AM number. ARF5 is expressed in the same temporal and spatial patterns as *AGO10* and activates *AGO10* expression through two ARE motifs in the *AGO10* promoter. Our findings do not necessarily contradict the conclusion that the initial formation of the AM stem cell niche requires an auxin minimum. The *ARF5* function uncovered in this study probably reflects a positive role of auxin at a later stage, i.e., during AM initiation, as we found that the *STM*-expressing stem cell niche is present in the *mps319* mutant that displays a strong AM deficiency. Another study indicates that *ARF5*, although expressed at a relatively low level in the SAM, promotes SAM formation and its subsequent development (Luo et al., 2018). Auxin and *ARF5* also organize the cambium meristem in the vasculature (Miyashima et al., 2019; Smetana et al., 2019). Together, these and our studies demonstrate the roles of auxin and *ARF5* in the patterning of various meristems.

BR is locally synthesized and promotes cell elongation through the loosening of the cell wall mainly in differentiated cells (Nemhauser et al., 2006; Symons and Reid, 2004). The function of BR in meristematic cells is much less known. *BZR1* was reported to repress *CUC3* expression at the boundary between the SAM and leaf primordia (Gendron et al., 2012). The AM phenotypes of *det2*, *bri1*, and *bzr1–1D* mutants led us to conclude that BR plays a negative role in AM development. *BZR1* represses *AGO10* expression through a BRRE motif in the *AGO10* promoter. Consistent with this negative role, *BZR1* expression is very low in AMs at the time of AM initiation (Figure 7I). However, after AM initiation, *BZR1* is expressed at a high level in developing AMs (Figure 4D), suggesting a potential role of *BZR1* in late stages of AM development, such as AM maintenance and lateral organ emergence in AMs.

Light is vital to plant morphogenesis. For example, mutants in the red/far-red light receptor *PHYB* display narrow, elongated leaf petioles and fewer branches (Finlayson et al., 2010). *PIF* genes promote hypocotyl elongation in the dark and are inactivated by *PHYB* upon light perception (Chen and Chory, 2011; Li et al., 2011). Given that AMs are embedded inside a plant, a role of light in AM initiation is not immediately obvious. The presence of a G-box in the *AGO10* promoter and the AM defects of *phyB* mutants led us to investigate the role of light in AM initiation. We found that *PIF4* overexpression inhibits AM initiation, and *PIF4* represses *AGO10* expression through the G-box. In contrast to *BZR1*, whose expression disappears at the time of AM initiation, the stable expression of *PIF4* on the adaxial side of young and old leaves implies that its negative role in AM initiation can be overcome by *ARF5* or unknown factors. AM initiation is probably determined by the relative quantities of the positive (*ARF5*) and negative (*PIF4*) factors.

In summary, we show that auxin, BR, and light converge on *AGO10* to coordinately regulate AM initiation. Crosstalk between hormones or between hormones and light is widely studied in developmental processes (Finlayson et al., 2010; Oh et al., 2014). However, the interaction between hormones and the miRNA pathway is little known. In AM development, *AGO10* integrates the developmental signals auxin and BR and the environmental signal light to impact miR165/166 activity. As AGO10 functions as a repressor of miR165/166 (Yu et al., 2017; Zhu et al., 2011), our work provides an example of intricate regulation of miRNA activity in a specific developmental process.

STAR★METHODS

RESOURCE AVAILABILITY

Lead Contact—Further information and requests for resources and reagents should be directed to and will be fulfilled by the Lead Contact, Xuemei Chen (xuemei.chen@ucr.edu).

Materials Availability—All unique/stable reagents generated in this study are available from the Lead Contact with a completed Materials Transfer Agreement.

Data and Code Availability—The raw imaging data have been deposited in Mendeley Data, under the link: https://data.mendeley.com/datasets/bhmtmgxdg5/draft?a=19337f63-a8c6-4e98-9c25-45290fd8129b. No new code was generated in this study.

EXPERIMENTAL MODEL AND SUBJECT DETAILS

Arabidopsis thaliana ecotypes Col-0, Ws, and Ler were used as wild-type controls. The *mp, mps319, mpΔ, pif4–2, phyB-9, bzr1–1D, det2, bri1–5, arf10, arf16, arf2, arf3, arf4, axr1, pif1, pif3, pif5, pifQ, p35S::AGO10* and *BES1 RNAi* lines are in the Col-0 background, the *pnh-2, phyB-5*, and *ago10–13* lines are in the Ler background and *pid-8* is in the Ws background (see Key Resources Table for references to these lines). Plants were grown in the greenhouse in soil at 22°C under short-day conditions (8 h light/16 h dark) for 28 to 30 d and were induced to flower under long-day conditions (16 h light/8 h dark) for 30 d unless otherwise specified.

For *pAGO10::GFPer* transgenic lines, *AGO10* promoter was amplified from *Arabidopsis* genomic DNA and inserted into the pMDC204 vector (Curtis and Grossniklaus, 2003). The plasmid was transformed into plants in Col background. *AGO10Δ* promoter was amplified by two or three fragments using corresponding primers (see Table S1) and assembled into the pMDC204 vector. The *pARF5::ARF5-GFP* construct was described before (Schlereth et al., 2010). The transgenic lines are crossed into the *mp* mutant (Berleth and Jurgens, 1993) and one line with lower levels of *ARF5* expression than wild type was identified to represent a weak *arf5* mutant.

The transgenic line *pARF5::ARF5-GFP mp-B4149*, in which the *pARF5::ARF5-GFP* transgene rescued the phenotypes of the *mp-B4149* allele (Schlereth et al., 2010), was used for imaging and ChIP analyses. For simplicity, the *ARF5::ARF5-GFP mp-B4149* line is referred to in the Results section as *ARF5::ARF5-GFP*. The *pARF5::ARF5-GFP* plasmid (Schlereth et al., 2010) was introduced into the Col background and one line with an obvious *ARF5* over expression phenotype (Krogan et al., 2012) was examined by qRT-PCR for overall (both endogenous and transgenic) *ARF5* transcript levels. This line was found to have higher *ARF5* expression and designated as an *ARF5* over expression (*ARF5 OX*) line. The transgenic lines were crossed with the *mp* mutant (Berleth and Jurgens, 1993) to generate *pARF5::ARF5-GFP mp*. One line only partially rescued the *mp* mutant phenotype and qRT-PCR showed that this line had lower levels of *ARF5* expression than wild type. Thus, this line was used to represent a weak *arf5* mutant.

A *pPIF4::PIF4-Citrine-HA pif4–101* transgenic line (Yamashino et al., 2013) was used for imaging and ChIP analyses. For simplicity, this line is referred to as *pPIF4::PIF4-Citrine-HA* in the Results section of the article. We crossed out the *pif4–101* mutation from this line so that the *pPIF4::PIF4-Citrine-HA* transgene was in the Col background. As the transgene caused obvious PIF4 over expression phenotypes, such as long hypocotyls (Yamashino et al., 2013), the *pPIF4::PIF4-Citrine-HA* line in the Col background was referred to as *PIF4 OX*.

pBZR1::*BZR1-CFP* and *pBZR1::BZR1m-CFP* were described before: *pBZR1::BZR1-CFP* can partially rescue the phenotypes of *bri1* mutants and is thus functional; *pBZR1::BZR1m-CFP* causes phenotypes similar to those of the *bzr1–1D* mutant, suggesting that it is constitutively active (Wang et al., 2002).

The *pAGO10D1* line was generated via genome editing. The guide RNA sequence was introduced into pCAMBIA1300-*pYAO*:-CAS9 (Yan et al., 2015) using primers

"ATTGCTGTAAAGACCAAGAATAAA" and "AAACTTTATTCTTGGTCTTTACAG". More than 20 T1 plants were obtained and plants in the T2 generation were genotyped. Three lines contained deletions covering the ARF5-binding site, and the line with the shortest deletion was chosen for further study. Homozygous plants with the deletion and without Cas9 were identified by genotyping and used for further analyses. For the generation of the *pAGO10Δ3*::*AGO10* and *pAGO10Δ4*::*AGO10* transgenic lines, the *AGO10Δ* promoters were each amplified in two fragments using corresponding primers (see Table S1) and assembled into the pCAMBIA1300 vector (Arabidopsis Biological Resource Center, Vector:6531241280). The *p35S::STTM165/166* transgenic line was described before (Yan et al., 2012) and the transgene was crossed into *ago10*.

METHOD DETAILS

Hormone Treatment and RT-PCR—For Dexamethasone (Dex) treatment, a 10mM stock solution of Dex (Sigma-Aldrich) in ethanol was diluted with distilled water to a final concentration of 10μM. Ethanol alone diluted in water was applied to leaf axils as the mock control. For other hormones, 50μM MeJA, 50μM IAA, 50μM ABA, 100μM ACC, 10μM GR24, 100 μM 6-BA, 100μM GA_3, and 10μM BL were incubated with boundary-enriched shoot apex for 3 hours or applied into leaf axils. For expression analyses, plants were grown for 21 d under short-day conditions and meristematic and boundary tissue was enriched by manual dissection to remove leaves from the shoot apex. Total RNA was extracted using the AxyPrep Multisource RNA Miniprep kit (Corning). First-strand cDNA synthesis was performed with 2μg total RNA, reverse transcriptase (Thermo Scientific) and a 22-mer oligo dT primer according to manufacturer's instructions. RT-PCR was performed in a 20μL reaction volume using Taq polymerase (Thermo Scientific) and gene-specific primers (Table S1). Quantitative RT-PCR was carried out in triplicate using iQ SYBRGreen Supermix (BioRad) on the BioRad CFX96 system. Values were obtained by normalizing to *UBQ10* or *TUB6* (Kaufmann et al., 2010; Zhang et al., 2018).

Tissue Preparation, Confocal Analysis and Scanning Electron Microscopy—Seedlings were grown in MS medium and in soil under short-day conditions (8 h light at 22°C and 16 h dark at 18°C) for 21d after seed stratification. Shoot apices were collected by removing the leaves, then immediately placed in 2.5% paraformaldehyde (PFA; Sigma-Aldrich) at pH 7.0 at 4°C, and vacuum-infiltrated for 30 min and stored overnight at 4°C. Fixed tissue samples were washed with 10% sucrose and 1% PFA at pH 7.0 for 20 min, with 20% sucrose and 1% PFA at pH 7.0 for 20 min, and 30% sucrose and 1% PFA at pH 7.0 for 30 min. Samples were then embedded in 5 to 7% low-melting-point agarose (Promega) liquid gel at 30°C and the liquid gel was incubated at 4°C for 15 min to solidify. Sections of 40 to 70 μm were made using an ELECTRON MICROSCOPY SCIENCES (EMS) vibratome tissue slicer.

Images were taken with a Leica SP5 microscope. GFP was excited using a 488 nm laser at 10–15% of its output, and the emission was 500–550 nm. Venus was excited using a 514 nm laser at 20–30% of its output, and the emission was 525–575 nm. Autofluorescence of chlorophyll was excited using 488 nm and 514 nm lasers at 10–15% and 20–30% of outputs, respectively, and detected at 650–700 nm (Shi et al., 2016).

The tissues from wild-type and mutant plants were dissected and immediately observed through a scanning electron microscope (Hitachi 4700).

Chromatin Immunoprecipitation and Realtime PCR—ChIP experiments were performed according to published protocols (Zhang et al., 2012). Shoots without leaves from ~28d short-day grown *pARF5::ARF5-GFP mp-B4149*, *pBZR1*::*BZR1-CFP* and *pPIF4::PIF4-Citrine-HA pif4–101* plants were harvested and fixed with 1% formaldehyde under vacuum for 10 min. Nuclei were isolated and lysed, and chromatin was sheared to a mean size of 1,000 bp by sonication. The sonicated chromatin served as an input. Immunoprecipitations were performed using an antibody against GFP (Sigma-Aldrich). The precipitated DNA was isolated, purified, and used as a template for PCR. qPCR was performed as described above (see Table S1 for primers). The data are presented as percentage of input. Three independent biological replicates were performed.

TRANSIENT EXPRESSION ASSAYS IN PROTOPLASTS

To produce the effector constructs, full-length *ARF5*, *BZR1* and *PIF4* open reading frames were amplified from *Arabidopsis* cDNA and inserted into the pBI221 vector under control of the CaMV *35S* promoter (Lin et al., 2007). The native *AGO10* promoter was amplified from *Arabidopsis* genomic DNA and the PCR fragment was inserted into the YY96 vector (Zhang et al., 2012) to produce *pAGO10::LUC*. For *pAGO10Δ::LUC,* fragments of promoter without binding motifs were amplified individually and assembled into the YY96 vector (see Table S1 for primers). The YY96 vector contained a CaMV *35S* minimal promoter before the *LUC* gene and a *p35S::REN* construct was recombined as internal control. Arabidopsis protoplasts were isolated from leaves of 14-day-old, short-day grown seedlings. Leaf strips were incubated in an enzyme solution (20mM MES, 1.5% cellulase R10, 0.75% macrozyme R10, 0.6M mannitol, 10mM KCl, 100mM CaCl2, 0.1%BSA) for 4h and then filter through a 35–75mm nylon mesh. The pellet was washed by the W5 solution (2mM MES, 154mM NaCl, 125 mM CaCl2, 5mM KCl), and resuspended in the MMg solution (4mM MES, 0.4M mannitol, 15mM MgCl2). The protoplasts were transfected using the PEG solution (20% PEG, 0.2M mannitol, 100mM CaCl2) (Zhang et al., 2012). The reporter construct containing internal control and effector plasmid were co-transformed into protoplasts. After transformation, the protoplasts were incubated at 23°C for 12–15 h. The protoplasts were pelleted and resuspended in 100 μL of 1 ×Cell Culture Lysis Reagent (CCLR) (Promega). For luciferase activity assays, 5 μL of the extract was mixed with 50 μL luciferase assay substrate (Promega), and the activity was detected using a Modulus Luminometer/ Fluorometer (Promega) and a luminescence kit (Promega). Reporter gene expression levels were expressed as firefly/Renilla luciferase activity ratios. Three independent experiments were each performed with three technical replicates.

QUANTIFICATION AND STATISTICAL ANALYSIS

Statistical parameters including the exact value of n, the definition of center, dispersion and precision measures (mean ± SD) and statistical significance were reported in the Figures and Figure Legends unless otherwise stated. Data was judged statistically significant when $P < 0.05$ by two-tailed unpaired Student's t-test. Significances are represented in the Figures as follows: **$p < 0.01$, unless individual p values were stated. Replicates in different

experiments were stated in corresponding Figure legends. Statistical analyses were performed in Excel and Origin 6.0.

Supplementary Material

Refer to Web version on PubMed Central for supplementary material.

ACKNOWLEDGMENTS

We thank Dr. Yanhai Yin at Iowa State University for *BES1* RnAi seeds, Dr. Xiaoya Chen at the Institute of Plant Physiology & Ecology, Shanghai Institutes for Biological Sciences for *arf* mutant seeds, Dr. Zhiyong Wang at the Carnegie Institute and Dr. Kang Chong at Institute of Botany, Chinese Academy of Sciences for BZR1-related seeds, Dr. Meng Chen at University of California, Riverside for PIF4-related and *phyB* mutant seeds, and Dr. Youfa Cheng at Institute of Botany, Chinese Academy of Sciences for *axr1–3* and *axr1–12* seeds. We also thank Yu Yu, Bailong Zhang, Yong Zhang, Chenjiang You, Yuan Wang, Tianran Jia, Shengben Li, Yonghui Zhao, and Zhenxia Su for technical assistance or discussions. This work was supported by NIH GM129373 to X.C. and NSFC 31870287 to B.M.

REFERENCES

Bao N, Lye KW, and Barton MK (2004). MicroRNA binding sites in Arabidopsis class III HD-ZIP mRNAs are required for methylation of the template chromosome. Dev. Cell 7, 653–662. [PubMed: 15525527]

Barton MK, and Poethig RS (1993). Formation of the shoot apical meristem in Arabidopsis-thaliana an analysis of development in the wild-type and in the shoot meristemless mutant. Development 119, 823–831.

Berleth T, and Jurgens G (1993). The role of the monopteros gene in organizing the basal body region of the Arabidopsis embryo. Development 118, 575–587.

Burian A, Barbier de Reuille P, and Kuhlemeier C (2016). Patterns of stem cell divisions contribute to plant longevity. Curr. Biol 26, 1385–1394. [PubMed: 27161504]

Carlsbecker A, Lee JY, Roberts CJ, Dettmer J, Lehesranta S, Zhou J, Lindgren O, Moreno-Risueno MA, Vatén A, Thitamadee S, et al. (2010). Cell signalling by microRNA165/6 directs gene dose-dependent root cell fate. Nature 465, 316–321. [PubMed: 20410882]

Chen M, and Chory J (2011). Phytochrome signaling mechanisms and the control of plant development. Trends Cell Biol. 21, 664–671. [PubMed: 21852137]

Chitwood DH, Nogueira FT, Howell MD, Montgomery TA, Carrington JC, and Timmermans MC (2009). Pattern formation via small RNA mobility. Genes Dev 23, 549–554. [PubMed: 19270155]

Chory J, Nagpal P, and Peto CA (1991). Phenotypic and genetic analysis of det2, a new mutant that affects light-regulated seedling development in Arabidopsis. Plant Cell 3, 445–459. [PubMed: 12324600]

Curtis MD, and Grossniklaus U (2003). A gateway cloning vector set for high-throughput functional analysis of genes in planta. Plant Physiol 133, 462–469. [PubMed: 14555774]

Dinneny JR, and Yanofsky MF (2004). Vascular patterning: xylem or phloem? Curr. Biol. 14, R112–R114. [PubMed: 14986642]

Finlayson SA, Krishnareddy SR, Kebrom TH, and Casal JJ (2010). Phytochrome regulation of branching in Arabidopsis. Plant Physiol. 152, 1914–1927. [PubMed: 20154098]

Gendron JM, Liu JS, Fan M, Bai MY, Wenkel S, Springer PS, Barton MK, and Wang ZY (2012). Brassinosteroids regulate organ boundary formation in the shoot apical meristem of Arabidopsis. Proc. Natl. Acad. Sci. USA 109, 21152–21157. [PubMed: 23213257]

Greb T, Clarenz O, Schafer E, Muller D, Herrero R, Schmitz G, and Theres K (2003). Molecular analysis of the lateral suppressor gene in Arabidopsis reveals a conserved control mechanism for axillary meristem formation. Genes Dev 17, 1175–1187. [PubMed: 12730136]

Guan C, Wu B, Yu T, Wang Q, Krogan NT, Liu X, and Jiao Y (2017). Spatial auxin signaling controls leaf flattening in Arabidopsis. Curr. Biol 27, 2940–2950.e4. [PubMed: 28943086]

He JX, Gendron JM, Sun Y, Gampala SSL, Gendron N, Sun CQ, and Wang ZY (2005). BZR1 is a transcriptional repressor with dual roles in brassinosteroid homeostasis and growth responses. Science 307, 1634–1638. [PubMed: 15681342]

Heisler MG, Ohno C, Das P, Sieber P, Reddy GV, Long JA, and Meyerowitz EM (2005). Patterns of auxin transport and gene expression during primordium development revealed by live imaging of the Arabidopsis inflorescence meristem. Curr. Biol 15, 1899–1911. [PubMed: 16271866]

Hibara K, Karim MR, Takada S, Taoka K, Furutani M, Aida M, and Tasaka M (2006). Arabidopsis cup-shaped COTYLEDON3 regulates postembryonic shoot meristem and organ boundary formation. Plant Cell 18, 2946–2957. [PubMed: 17122068]

Huq E, and Quail PH (2002). PIF4, a phytochrome-interacting bHLH factor, functions as a negative regulator of phytochrome B signaling in Arabidopsis. EMBO J 21, 2441–2450. [PubMed: 12006496]

Ji LJ, Liu XG, Yan J, Wang WM, Yumul RE, Kim YJ, Dinh TT, Liu J, Cui X, Zheng BL, et al. (2011). ARGONAUTE10 and ARGONAUTE1 regulate the termination of floral stem cells through two microRNAs in Arabidopsis. PLoS Genet 7, e1001358. [PubMed: 21483759]

Juarez MT, Kui JS, Thomas J, Heller BA, and Timmermans MC (2004). MicroRNA-mediated repression of rolled leaf1 specifies maize leaf polarity. Nature 428, 84–88. [PubMed: 14999285]

Kaufmann K, Wellmer F, Muiño JM, Ferrier T, Wuest SE, Kumar V, Serrano-Mislata A, Madueño F, Krajewski P, Meyerowitz EM, et al. (2010). Orchestration of floral initiation by APETALA1. Science 328, 85–89. [PubMed: 20360106]

Krogan NT, Ckurshumova W, Marcos D, Caragea AE, and Berleth T (2012). Deletion of MP/ARF5 domains III and IV reveals a requirement for Aux/IAA regulation in Arabidopsis leaf vascular patterning. New Phytol 194, 391–401. [PubMed: 22320407]

Leduc N, Roman H, Barbier F, Péron T, Huché-Thélier L, Lothier J, Demotes-Mainard S, and Sakr S (2014). Light signaling in bud outgrowth and branching in plants. Plants (Basel) 3, 223–250. [PubMed: 27135502]

Leivar P, Monte E, Oka Y, Liu T, Carle C, Castillon A, Huq E, and Quail PH (2008). Multiple phytochrome-interacting bHLH transcription factors repress premature seedling photomorphogenesis in darkness. Curr. Biol 18, 1815–1823. [PubMed: 19062289]

Li J, Li G, Wang H, and Wang Deng X (2011). Phytochrome signaling mechanisms. Arabidopsis Book 9, e0148. [PubMed: 22303272]

Li JM, Biswas MG, Chao A, Russell DW, and Chory J (1997). Conservation of function between mammalian and plant steroid 5 alpha-reductases. Proc. Natl. Acad. Sci. USA 94, 3554–3559. [PubMed: 9108014]

Li QF, Lu J, Yu JW, Zhang CQ, He JX, and Liu QQ (2018). The brassinosteroid-regulated transcription factors BZR1/BES1 function as a coordinator in multisignal-regulated plant growth. Biochim. Biophys. Acta Gene Regul. Mech 1861, 561–571. [PubMed: 29673687]

Lin R, Ding L, Casola C, Ripoll DR, Feschotte C, and Wang H (2007). Transposase-derived transcription factors regulate light signaling in Arabidopsis. Science 318, 1302–1305. [PubMed: 18033885]

Liu Q, Yao X, Pi L, Wang H, Cui X, and Huang H (2009). The ARGONAUTE10 gene modulates shoot apical meristem maintenance and establishment of leaf polarity by repressing miR165/166 in Arabidopsis. Plant J 58, 27–40. [PubMed: 19054365]

Luo L, Zeng J, Wu H, Tian Z, and Zhao Z (2018). A molecular framework for auxin-controlled homeostasis of shoot stem cells in Arabidopsis. Mol. Plant 11, 899–913. [PubMed: 29730265]

Lynn K, Fernandez A, Aida M, Sedbrook J, Tasaka M, Masson P, and Barton MK (1999). The PINHEAD/ZWILLE gene acts pleiotropically in Arabidopsis development and has overlapping functions with the ARGONAUTE1 gene. Development 126, 469–481. [PubMed: 9876176]

Mallory AC, Reinhart BJ, Jones-Rhoades MW, Tang G, Zamore PD, Barton MK, and Bartel DP (2004). MicroRNA control of PHABULOSA in leaf development: importance of pairing to the microRNA 5′ region. EMBO J 23, 3356–3364. [PubMed: 15282547]

Mcconnell JR, and Barton MK (1995). Effect of mutations in the pinhead gene of Arabidopsis on the formation of shoot apical meristems. Dev. Genet. 16, 358–366.

Miyashima S, Roszak P, Sevilem I, Toyokura K, Blob B, Heo JO, Mellor N, Help-Rinta-Rahko H, Otero S, Smet W, et al. (2019). Mobile PEAR transcription factors integrate positional cues to prime cambial growth. Nature 565, 490–494. [PubMed: 30626969]

Müller D, Schmitz G, and Theres K (2006). Blind homologous R2R3 Myb genes control the pattern of lateral meristem initiation in Arabidopsis. Plant Cell 18, 586–597. [PubMed: 16461581]

Nemhauser JL, Hong F, and Chory J (2006). Different plant hormones regulate similar processes through largely nonoverlapping transcriptional responses. Cell 126, 467–475. [PubMed: 16901781]

Noguchi T, Fujioka S, Choe S, Takatsuto S, Yoshida S, Yuan H, Feldmann KA, and Tax FE (1999). Brassinosteroid-insensitive dwarf mutants of Arabidopsis accumulate brassinosteroids. Plant Physiol 121, 743–752. [PubMed: 10557222]

Oh E, Zhu JY, Bai MY, Arenhart RA, Sun Y, and Wang ZY (2014). Cell elongation is regulated through a central circuit of interacting transcription factors in the Arabidopsis hypocotyl. eLife 3.

Otsuga D, DeGuzman B, Prigge MJ, Drews GN, and Clark SE (2001). REVOLUTA regulates meristem initiation at lateral positions. Plant J 25, 223–236. [PubMed: 11169198]

Raman S, Greb T, Peaucelle A, Blein T, Laufs P, and Theres K (2008). Interplay of miR164, CUP-SHAPED COTYLEDON genes and LATERAL SUPPRESSOR controls axillary meristem formation in Arabidopsis thaliana. Plant J 55, 65–76. [PubMed: 18346190]

Schlereth A, Möller B, Liu W, Kientz M, Flipse J, Rademacher EH, Schmid M, Jürgens G, and Weijers D (2010). MONOPTEROS controls embryonic root initiation by regulating a mobile transcription factor. Nature 464, 913–916. [PubMed: 20220754]

Shi BH, Zhang C, Tian CH, Wang J, Wang Q, Xu TF, Xu Y, Ohno C, Sablowski R, Heisler MG, et al. (2016). Two-step regulation of a meristematic cell population acting in shoot branching in Arabidopsis. PLoS Genet. 12, e1006168. [PubMed: 27398935]

Shuai B, Reynaga-Peña CG, and Springer PS (2002). The lateral organ boundaries gene defines a novel, plant-specific gene family. Plant Physiol 129, 747–761. [PubMed: 12068116]

Smetana O, Mäkilä R, Lyu M, Amiryousefi A, Sánchez Rodríguez F, Wu MF, Solé-Gil A, Leal Gavarrón M, Siligato R, Miyashima S, et al. (2019). High levels of auxin signalling define the stem-cell organizer of the vascular cambium. Nature 565, 485–489. [PubMed: 30626967]

Symons GM, and Reid JB (2004). Brassinosteroids do not undergo long-distance transport in pea. Implications for the regulation of endogenous brassinosteroid levels. Plant Physiol 135, 2196–2206. [PubMed: 15299131]

Talbert PB, Adler HT, Parks DW, and Comai L (1995a). The revoluta gene is necessary for apical meristem development and for limiting cell divisions in the leaves and stems of Arabidopsis thaliana. Development 121, 2723–2735. [PubMed: 7555701]

Talbert PB, Adler HT, Parks DW, and Comai L (1995b). The REVOLUTA gene is necessary for apical meristem development and for limiting cell divisions in the leaves and stems of Arabidopsis thaliana. Development 121, 2723–2735. [PubMed: 7555701]

Tatematsu K, Toyokura K, Miyashima S, Nakajima K, and Okada K (2015). A molecular mechanism that confines the activity pattern of miR165 in Arabidopsis leaf primordia. Plant J 82, 596–608. [PubMed: 25788175]

Tucker MR, Hinze A, Tucker EJ, Takada S, Jürgens G, and Laux T (2008). Vascular signalling mediated by ZWILLE potentiates WUSCHEL function during shoot meristem stem cell development in the Arabidopsis embryo. Development 135, 2839–2843. [PubMed: 18653559]

Ulmasov T, Liu ZB, Hagen G, and Guilfoyle TJ (1995). Composite structure of auxin response elements. Plant Cell 7, 1611–1623. [PubMed: 7580254]

Vernoux T, Brunoud G, Farcot E, Morin V, Van den Daele H, Legrand J, Oliva M, Das P, Larrieu A, Wells D, et al. (2011). The auxin signaling network translates dynamic input into robust patterning at the shoot apex. Mol. Syst. Biol 7, 508. [PubMed: 21734647]

Wang JW, Wang LJ, Mao YB, Cai WJ, Xue HW, and Chen XY (2005). Control of root cap formation by microRNA-targeted auxin response factors in Arabidopsis. Plant Cell 17, 2204–2216. [PubMed: 16006581]

Wang Q, Kohlen W, Rossmann S, Vernoux T, and Theres K (2014a). Auxin depletion from the leaf axil conditions competence for axillary meristem formation in Arabidopsis and tomato. Plant Cell 26, 2068–2079. [PubMed: 24850851]

Wang Y, Wang J, Shi B, Yu T, Qi J, Meyerowitz EM, and Jiao Y (2014b). The stem cell niche in leaf axils is established by auxin and cytokinin in Arabidopsis. Plant Cell 26, 2055–2067. [PubMed: 24850849]

Wang ZY, Nakano T, Gendron J, He J, Chen M, Vafeados D, Yang Y, Fujioka S, Yoshida S, Asami T, et al. (2002). Nuclear-localized BZR1 mediates brassinosteroid-induced growth and feedback suppression of brassinosteroid biosynthesis. Dev. Cell 2, 505–513. [PubMed: 11970900]

Yamashino T, Nomoto Y, Lorrain S, Miyachi M, Ito S, Nakamichi N, Fankhauser C, and Mizuno T (2013). Verification at the protein level of the PIF4-mediated external coincidence model for the temperature-adaptive photoperiodic control of plant growth in Arabidopsis thaliana. Plant Signal. Behav 8, e23390. [PubMed: 23299336]

Yan J, Gu Y, Jia X, Kang W, Pan S, Tang X, Chen X, and Tang G (2012). Effective small RNA destruction by the expression of a short tandem target mimic in Arabidopsis. Plant Cell 24, 415–427. [PubMed: 22345490]

Yan L, Wei S, Wu Y, Hu R, Li H, Yang W, and Xie Q (2015). High-efficiency genome editing in Arabidopsis using YAO promoter-driven CRISPR/Cas9 system. Mol. Plant 8, 1820–1823. [PubMed: 26524930]

Yin Y, Vafeados D, Tao Y, Yoshida S, Asami T, and Chory J (2005). A new class of transcription factors mediates brassinosteroid-regulated gene expression in Arabidopsis. Cell 120, 249–259. [PubMed: 15680330]

Yu Y, Ji LJ, Le BH, Zhai JX, Chen JY, Luscher E, Gao L, Liu CY, Cao XF, Mo BX, et al. (2017). ARGONAUTE10 promotes the degradation of miR165/6 through the SDN1 and SDN2 exonucleases in Arabidopsis. PLoS Biol 15, e2001272. [PubMed: 28231321]

Zhang C, Wang J, Wenkel S, Chandler JW, Werr W, and Jiao YL (2018). Spatiotemporal control of axillary meristem formation by interacting transcriptional regulators. Development 145.

Zhang C, Xu Y, Guo S, Zhu J, Huan Q, Liu H, Wang L, Luo G, Wang X, and Chong K (2012). Dynamics of brassinosteroid response modulated by negative regulator LIC in rice. PLoS Genet 8, e1002686. [PubMed: 22570626]

Zhu H, Hu F, Wang R, Zhou X, Sze SH, Liou LW, Barefoot A, Dickman M, and Zhang X (2011). Arabidopsis Argonaute10 specifically sequesters miR166/165 to regulate shoot apical meristem development. Cell 145, 242–256. [PubMed: 21496644]

Highlights

- *AGO10* promotes AM initiation by promoting *REV* and *STM* expression
- *AGO10* expression is spatiotemporally coincidental with AM initiation
- Auxin, brassinosteroids, and light converge on *AGO10* to regulate AM initiation
- *AGO10* expression patterns are specified by *ARF5*, *BZR1*, and *PIF4*

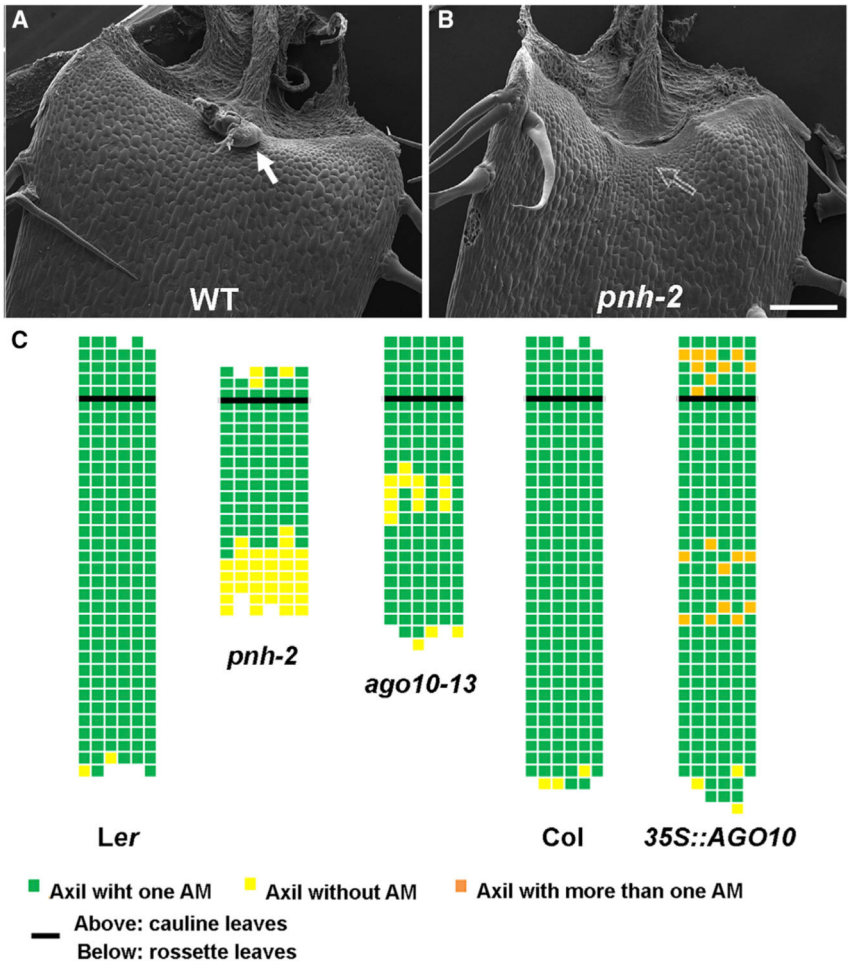

Figure 1. ***ago10*** **Mutants Show AM Defects**

(A and B) Scanning electron micrographs of the basal regions of stage P_{17} rosette leaves showing an axillary bud (solid arrow) in the leaf axil in wild type (A) and the absence of an axillary bud (dotted arrow) in the *pnh-2* mutant (B). Bars, 100 μm.

(C) Schematic representation of AM phenotypes in wild type (Ler and Col), *pnh-2*, *ago10–13*, and *p35S::AGO10* plants. Note that *pnh-2* and *ago10–13* are in the Ler background while *p35S::AGO10* is in the Col background. The black horizontal line represents the border between the youngest rosette leaf and the oldest cauline leaf. Each column represents a single plant, and each square within a column represents an individual leaf axil. The bottom row represents the oldest rosette leaf, with progressively younger leaves above. The color green indicates the presence of an axillary bud, yellow indicates the absence of an axillary bud and orange indicates more than one axillary bud in one leaf axil.

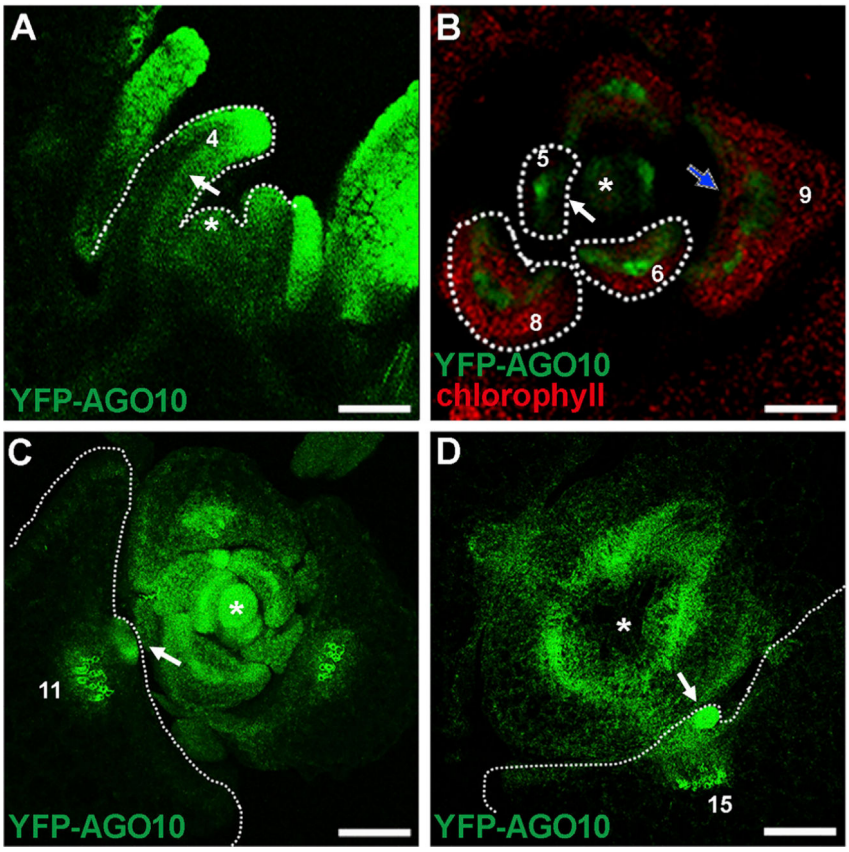

Figure 2. *AGO10* Is Expressed on the Adaxial Side of Young Leaves and in Axillary Meristems

Shoot apices of *pZLL::YFP-ZLL zll-1* plants were sectioned and imaged for YFP-ZLL (YFP-AGO10) signals. The numbers indicate the developmental stages of leaves. Asterisks represent the SAM. Bars, 50 μm.

(A) A longitudinal section showing that YFP-AGO10 signals are on the adaxial side of young leaves P_4.

(B) A cross section showing YFP-AGO10 signals on the adaxial side of young leaves (P_5) and in the middle zone in older leaves (P_6 and P_8). YFP-AGO10 signals begin to appear on the adaxial side of P_9 (blue arrow). The green color represents YFP-AGO10 signals and the red color indicates auto fluorescence from chloroplasts.

(C) A cross section showing YFP-AGO10 signals in the first initiated AM (arrow) in the axil of a P_{11} leaf.

(D) A cross section showing YFP-AGO10 signals in an axillary bud developed from an AM (arrow) in the axil of a P_{15} leaf.

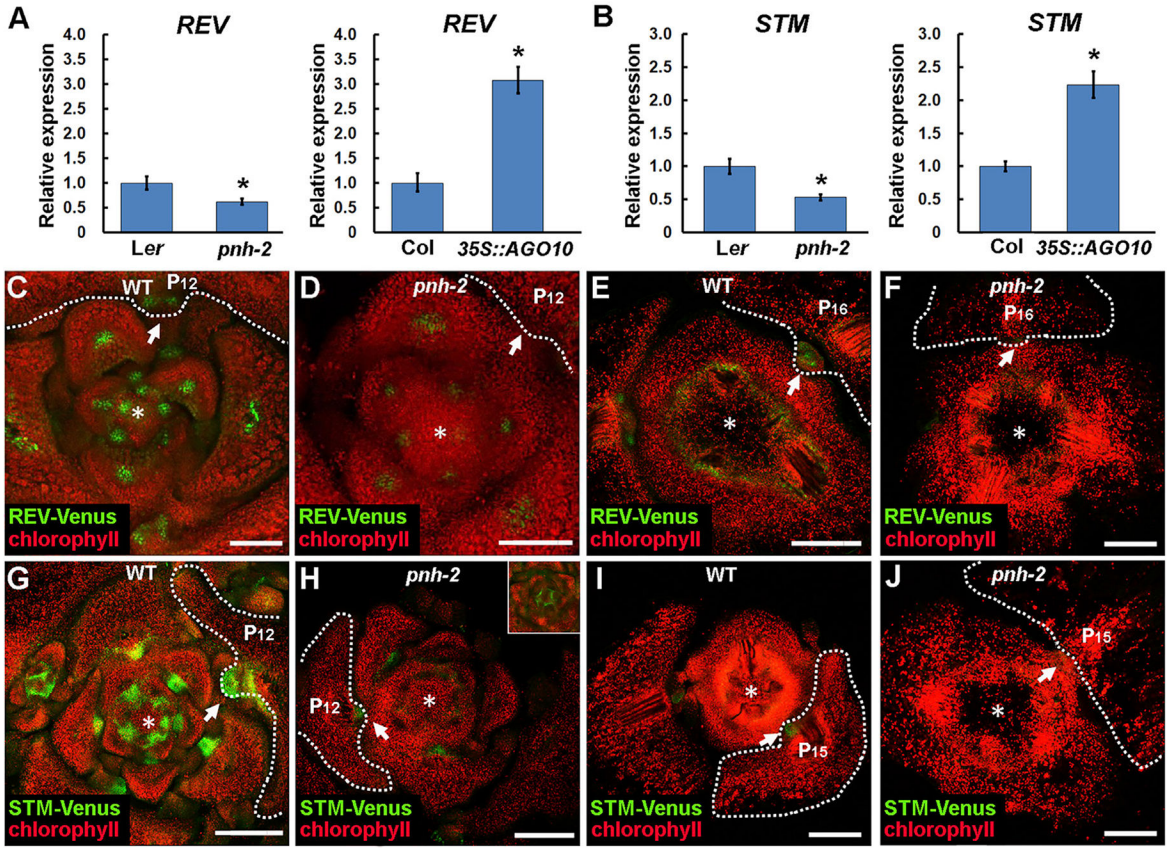

Figure 3. *AGO10* Promotes *REV* and *STM* Expression

(A and B) *REV* (A) and *STM* (B) expression levels in wild type, *pnh-2*, and an *AGO10* overexpression line (*p35S::AGO10*) as determined by qRT-PCR. Error bars represent SD from three independent replicates. *p < 0.01, (Student's t test).

(C–F) Cross sections of shoot apices from *pREV::REV-Venus* (C and E) and *pREV::REV-Venus pnh-2* (D and F). REV-Venus signals are present in the AM (arrow) at the axil of a P_{12} leaf in wild type (C). REV-Venus signals are extremely low in *pREV::REV-Venus pnh-2* throughout the apex including at the axil of a P_{12} leaf (D). REV-Venus signals are present in a larger AM in the axil of a P_{16} leaf in *pREV::REV-Venus* (E) but not in the axil of a leaf of a similar stage in *pREV::REV-Venus pnh-2* (F).

(G–J) Cross sections of shoot apices from *pSTM::STM-Venus* (G and I) and *pSTM::STM-Venus pnh-2* (H and J) plants. STM-Venus signals are present in AMs (arrows) in the axils of P_{12} (G) and P_{15} (I) leaves in *pSTM::STM-Venus*. The signals in the corresponding leaf axils are extremely low in *pSTM::STM-Venus pnh-2* (H and J). Note that STM-Venus signals in the axils of young leaves near the SAM in (G) and (H) cannot be directly compared, as the section in (H) does not capture the SAM/leaf boundaries due to morphological differences between *pnh-2* and wild type. The inset in (H) shows the SAM/leaf boundaries with STM-Venus signals in young leaf axils in *pnh-2*. The most drastic difference in *STM-Venus* expression between wild type and *pnh-2* is in axils of P_{11} and older leaves. Bars, 50 μm in (C–J). Asterisks indicate the SAM.

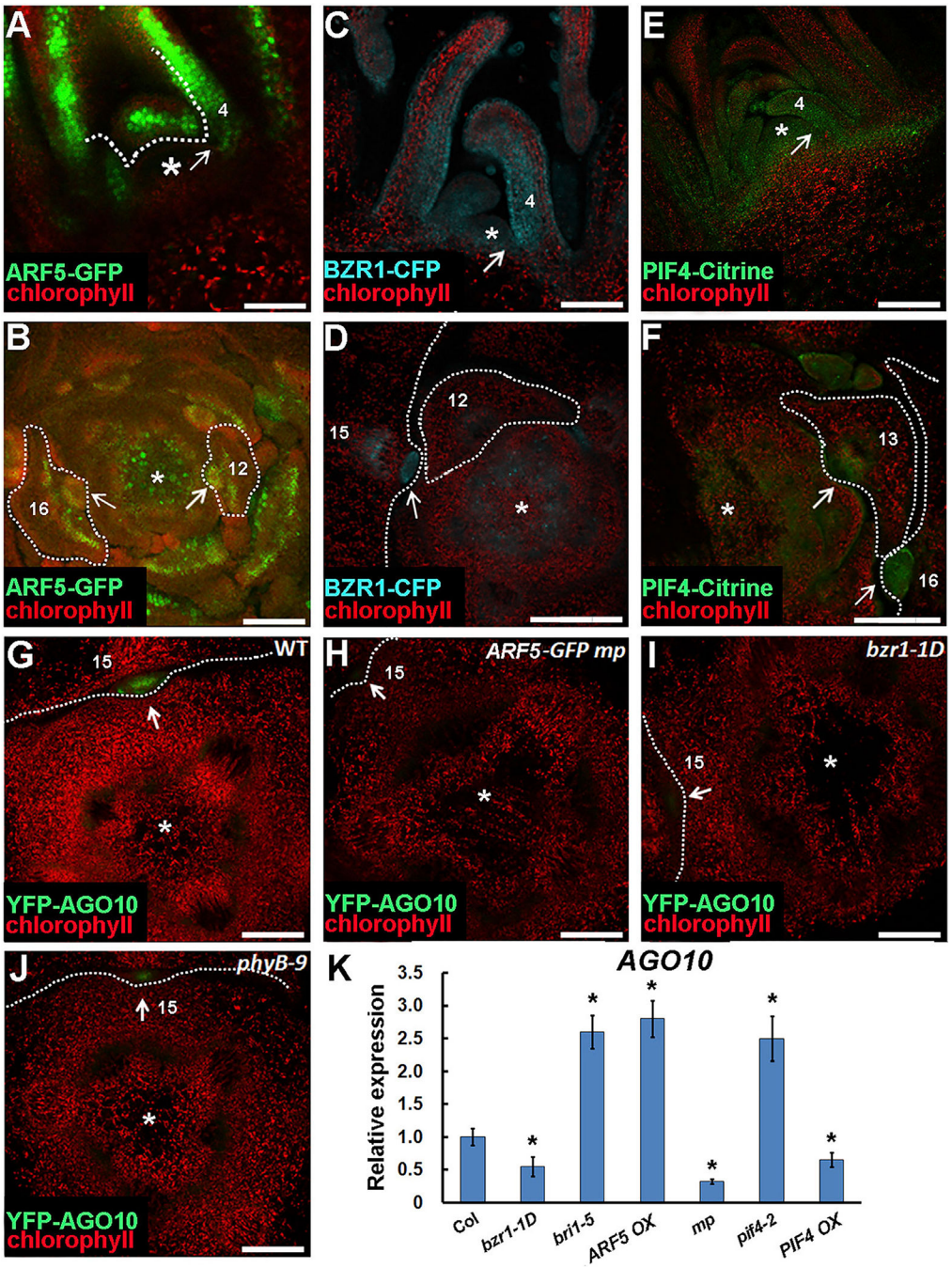

Figure 4. *ARF5*, *BZR1*, and *PIF4* Expression Patterns at the Shoot Apex in Wild Type and *AGO10* Expression in Various Mutants

Asterisks indicate the SAM, and the numbers indicate the developmental stages of leaves. Bars, 50 μm in (A–J).

(A and B) Longitudinal (A) and cross (B) sections of shoot apices of *pARF5::ARF5-GFP* plants. ARF5-GFP signals are present on the adaxial side of young leaves (P_4) and at the leaf/SAM boundary (arrow) (A). ARF5-GFP signals are present in AMs (arrows in B).

(C and D) Longitudinal (C) and cross (D) sections of shoot apices of *pBZR1::BZR1-CFP* plants. BZR1-CFP signals are found on the adaxial side of young leaves and at the leaf/SAM boundary (arrow) (C) and in AMs (arrow) (D).

(E and F) Longitudinal (E) and cross (F) sections of shoot apices of *pPIF4::PIF4-Citrine-HA* plants. PIF4-Citrine signals are found on the adaxial side of young leaves and at the leaf/SAM boundary (arrow) (E) and in AMs (arrow) (F).

(G–J) Cross sections of shoot apices from plants of various genotypes showing YFP-AGO10 signals in axils of P_{15} leaves. The *pAGO10::YFP-AGO10* transgene in wild type (G) was introduced into *ARF5-GFP mp* (H), *bzr-1D* (I), and *phyB-9* (J) through crosses. Note that *pARF5::ARF5-GFP mp* is considered a weak *arf5* allele due to lower levels of *ARF5* expression than wild type.

(K) qRT-PCR analysis to determine *AGO10* transcript levels in Col (wild type) and various other genotypes as indicated. Error bars indicate the SD of three independent replicates. Transcript levels were compared with those in Col. *$p < 0.01$, (Student's t test).

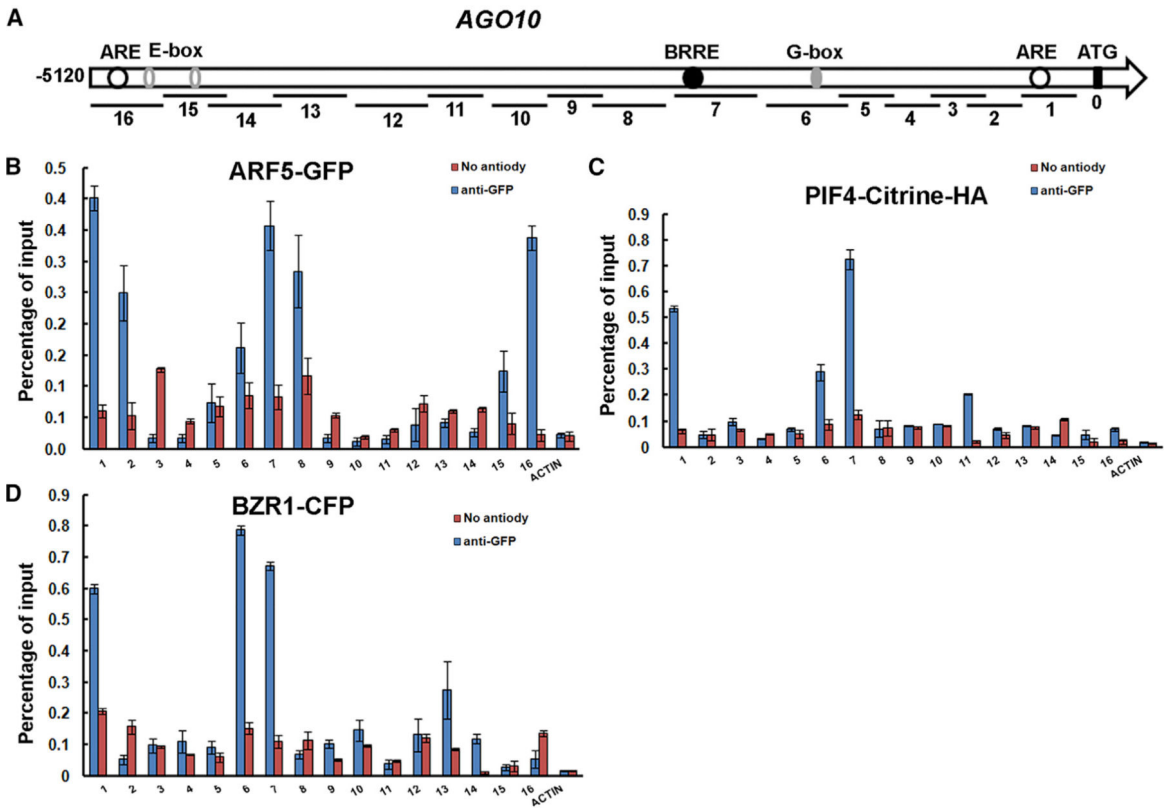

Figure 5. ARF5, PIF4, and BZR1 Bind the *AGO10* Promoter to Directly Regulate *AGO10* Expression

(A) Schematic representation of the *AGO10* promoter showing the positions of various motifs. ARE, auxin response elements; BRRE, brassinosteroid response element; G-box, a motif with high affinity for PIF4; E-box, a motif with low affinity for PIF4. ATG denotes the translation start site. Sixteen PCR fragments were designed for ChIP analysis.

(B–D) ChIP-qPCR analysis to determine the binding of ARF5-GFP (B), PIF4-Citrine-HA (C), and BZR1-CFP (D) to the *AGO10* promoter. Error bars indicate the SD of three independent replicates.

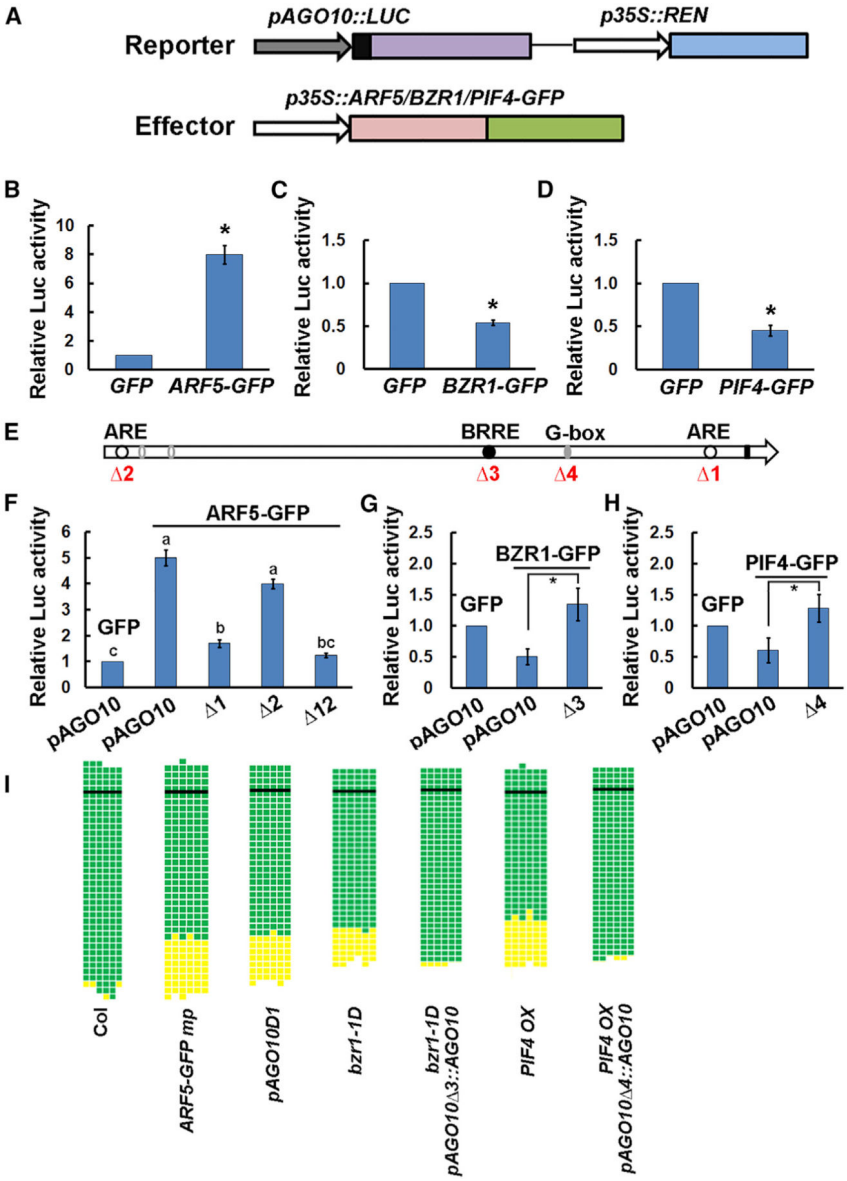

Figure 6. *ARF5*, *BZR1*, and *PIF4* Regulate *AGO10* Transcription to Influence AM Forma-tion

(A) Schematic diagrams of the luciferase reporter (*pAGO10::LUC*), the internal control (*p35S::REN*), and the effectors used in transient expression assays in *Arabidopsis* protoplasts. The reporter gene *LUC* was driven by the *AGO10* promoter (a 5120-bp region upstream of the ATG diagramed in Figure 5A). A minimal *35S* promoter was included 3′ of the *AGO10* promoter (black square). Renila luciferase was driven by the *35S* promoter. The effector was *ARF5-GFP*, *BZR1-GFP*, or *PIF4-GFP* driven by the *35S* promoter. The GFP vector alone served as a negative control.

(B–D) Relative *LUC* expression in transcriptional activity assays in Arabidopsis protoplasts. The reporter was co-transformed with the empty vector *p35S::GFP* or one of the effectors *p35S::ARF5/BZR1/PIF4-GFP* constructs. Data are means ± SD for three independent experiments, each performed in triplicate. *p < 0.01.

(E) A schematic diagram showing the deleted sites in the *AGO10* promoter.

(F) Relative (firefly/Renilla) luciferase activity in protoplasts co-transformed with *p35S*::*ARF5-GFP* or *p35S::GFP*, and the reporters driven by the native *AGO10* promoter (*pAGO10*) or promoters with one (Δ1, Δ2) or both (Δ12) AREs deleted. Data are mean ± SD for three independent experiments, each performed in triplicate. One-way ANOVA and post hoc Tukey testing were used for statistical analysis. Different letters indicate significantly different values ($p < 0.05$).

(G) Relative(firefly/Renilla) luciferase activity in protoplasts co-transformed with *p35S*::*BZR1-GFP* or *p35S::GFP*, and the reporters driven by the native *AGO10* promoter (*pAGO10*) or the promoter with the BRRE deleted (Δ3). *$p < 0.01$, (Student's t test).

(H) Relative (firefly/Renilla) luciferase activity in protoplasts co-transformed with *p35S*::*PIF4-GFP* or *p35S::GFP*, and the reporters driven by the native *AGO10* promoter (*pAGO10*) or the promoter with the G-box deleted (Δ4). *$p < 0.01$, (Student's t test).

(I) AM phenotypes of the indicated genotypes that were generated to interrogate the genetic relationships between auxin/light/BR and *AGO10*. Note that *pAGO10D1* is a line with a deletion of the ARF5-binding site in the *AGO10* promoter generated by Crispr-Cas9. *pAGO10D1* showed AM defects in early leaves. *AGO10* expression driven by the BZR1-binding-site-deleted promoter (*pAGO10Δ3*) and the PIF4-binding-site-deleted promoter (*pAGO10Δ4*) rescued the AM defects in *bzr1–1D* and *PIF4 OX*, respectively.

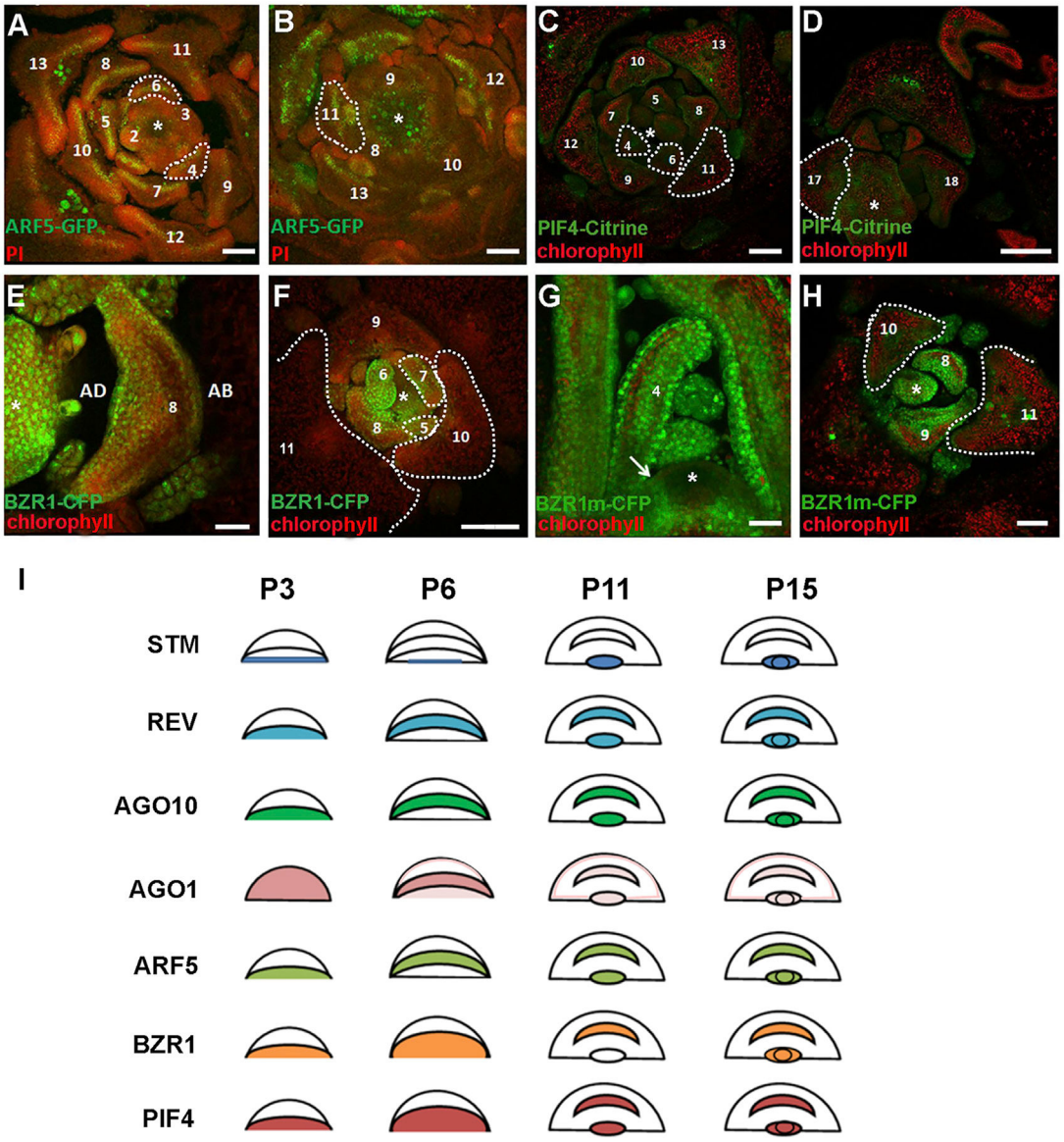

Figure 7. *ARF5, PIF4,* and *BZR1* Exhibit Different Temporal and Spatial Patterns of Expression during AM Development

(A–F, G, and H) Cross (A–F and H) and longitudinal (G) sections of shoot apices show the signals of fluorescent protein-tagged ARF5, PIF4, and BZR1. Numbers represent the developmental stages of leaves. AD, adaxial side; AB, abaxial side. Bars, 100 μm.

(A and B) Cross sections of shoot apices of *pARF5::ARF5-GFP* plants. ARF5-GFP signals are on the adaxial side of young leaves (P_4), in the middle zone in older leaves before AM initiation (P_6, A) and in AMs in mature leaf axils (P_{11}, B).

(C and D) Cross sections of shoot apices of *pPIF4::PIF4-Citrine-HA* plants. PIF4-Citrine signals are on the adaxial side of both young (P_4 and P_6 in C) and mature (P_{11} in C and P_{17} in D) leaves.

(E and F) Cross sections of shoot apices of *pBZR1::BZR1-CFP* plants. BZR1-CFP accumulates in a high-to-low gradient from the adaxial side to the abaxial side in young

leaves (P_8 in E); it is localized more in the nucleus on the adaxial side and more in the cytoplasm on the abaxial side. BZR1-CFP accumulates to higher levels in the epidermis (E). Temporally, BZR1-CFP is present in young leaves before AM initiation (P_5–P_7 in F) and absent in mature leaves immediately before or during AMs initiation (P_{10} and P_{11} in F).
(G and H) Longitudinal (G) and cross (H) sections of apices of *pBZR1::BZR1m-CFP* plants (a phosphorylation site in BZR1 is mutated in BZR1m). BZR1m-CFP signals are on the adaxial side and in the epidermis of young leaves (P_8–P_{10} in H). BZR1m-CFP signals persist in leaf stages when AMs would initiate ($P_{11,}$ H).
(I) Diagrams of gene expression patterns during AM development. P_3, P_6, and P_{11} represent newly emerged leaf primordium, leaf primordium beginning to develop the vasculature, and an older leaf with AM initiation in its axil, respectively. *STM* is expressed in the P_3 leaf/SAM boundary; its expression decreases at the P_6/SAM boundary and begins to increase in the axil of P_{11}. *REV*, *AGO10*, and *ARF5* are expressed on the adaxial side of P_3, in the middle zone as the leaves develop the vasculature and eventually in the vasculature and in the center of leaf axils where AMs initiate. *AGO1* is expressed throughout P_3, predominantly in the middle zone, epidermis, and on the adaxial side of P_6 and in the vasculature, epidermis, and AMs in P_{11}. *BZR1* is expressed on the adaxial side of P_3 and P_6, and in the vasculature in P_{11}. *PIF4* expression persists on the adaxial side of all leaves and appears in the vasculature in P_{11}. After AM initiation, all the genes are expressed in axillary buds of P_{15} with specific patterns not depicted in the diagrams.

KEY RESOURCES TABLE

REAGENT or RESOURCE	SOURCE	IDENTIFIER
Antibodies		
Rabbit polyclonal anti-HA	Sigma	Cat#H6908
Rabbit polyclonal anti-GFP	ABCAM	Cat#AB290
Chemicals		
1-aminocyclopropane-1-carboxylic acid (ACC)	Sigma	Cat#A3903
Jasmonic acid (JA)	Sigma	Cat#J2500
Abscicic acid (ABA)	Sigma	Cat#A1049
Indole-3-acetic acid (IAA)	Sigma	Cat#I2886
6-benzylaminopurine (BAP)	Sigma	Cat#B3408
epibrassinolide (eBL)	Sigma	Cat#E1641
Cycloheximide (CHX)	MP	Cat#100183
Dexamethasone (Dex)	Sigma	Cat#D1756
Propidium iodide (PI)	Sigma	Cat# P4170
Toluidine Blue O (TBO)	Sigma	Cat# T3260
Experimental Models: Organisms/Strains		
Arabidopsis thaliana: *arf5–2*	Arabidopsis Biological Resource Center	SALK_021319
Arabidopsis thaliana: *mp*	Arabidopsis Biological Resource Center	CS8147
Arabidopsis thaliana: *mpΔ*	Krogan et al., 2012	N/A
Arabidopsis thaliana: *arf5–1*	Arabidopsis Biological Resource Center	SALK_023812
Arabidopsis thaliana: *pARF5::ARF5-GFP mp-B4149*	Schlereth et al., 2010	N/A
Arabidopsis thaliana: *pARF5::ARF5-GFP* (*ARF5 OX*)	This Paper	N/A
Arabidopsis thaliana: *pARF5::ARF5-GFP mp*	This Paper	N/A
Arabidopsis thaliana: *arf2–6*	Arabidopsis Biological Resource Center	CS24600
Arabidopsis thaliana: *arf3–2*	Arabidopsis Biological Resource Center	SALK_005658C
Arabidopsis thaliana: *arf4–1*	Arabidopsis Biological Resource Center	SALK_023804C
Arabidopsis thaliana: *arf16–2*	Arabidopsis Biological Resource Center	SALK_021448
Arabidopsis thaliana: *arf10–2*	Wang et al., 2005	N/A
Arabidopsis thaliana: *pid-8*	Arabidopsis Biological Resource Center	CS69064
Arabidopsis thaliana: *axr1–3*	Arabidopsis Biological Resource Center	CS3075
Arabidopsis thaliana: *axr1–12*	Arabidopsis Biological Resource Center	CS3076
Arabidopsis thaliana: *bri1–5*	Noguchi et al., 1999	N/A
Arabidopsis thaliana: *det2*	Chory et al., 1991	N/A

REAGENT or RESOURCE	SOURCE	IDENTIFIER
Arabidopsis thaliana: *bzr1–1D*	Arabidopsis Biological Resource Center	CS65987
Arabidopsis thaliana: *BES1 RNAi*	Yin et al., 2005	N/A
Arabidopsis thaliana: *pBZR1::BZR1-CFP*	Wang et al., 2002	N/A
Arabidopsis thaliana: *pBZR1::BZR1m-CFP*	Wang et al., 2002	N/A
Arabidopsis thaliana: *pif4–2*	Arabidopsis Biological Resource Center	CS66043
Arabidopsis thaliana: *phyB-5*	Arabidopsis Biological Resource Center	CS6213
Arabidopsis thaliana: *phyB-9*	Arabidopsis Biological Resource Center	CS6217
Arabidopsis thaliana: *pPIF4::PIF4-Citrine-HA pif4–101*	Yamashino et al., 2013	N/A
Arabidopsis thaliana: *pPIF4::PIF4-Citrine-HA* (*PIF4 OX*)	Yamashino et al., 2013 This paper	N/A
Arabidopsis thaliana: *pif1–1*	Arabidopsis Biological Resource Center	CS66041
Arabidopsis thaliana: *pif3–3*	Arabidopsis Biological Resource Center	CS71665
Arabidopsis thaliana: *pifQ*	Arabidopsis Biological Resource Center	CS66049
Arabidopsis thaliana: *pif5–3*	Arabidopsis Biological Resource Center	CS66044
Arabidopsis thaliana: *pZLL::YFP-ZLL zll-1*	Tucker et al., 2008	N/A
Arabidopsis thaliana: *p35S::STTM165/166*	Yan et al., 2012	N/A
Arabidopsis thaliana: *pAGO10::GFPer*	This Paper	N/A
Arabidopsis thaliana: *pAGO10Δ1::GFPer*	This Paper	N/A
Arabidopsis thaliana: *pAGO10Δ34:GFPer*	This Paper	N/A
Arabidopsis thaliana: *pAGO10Δ3::AGO10*	This Paper	N/A
Arabidopsis thaliana: *pAGO10Δ4::AGO10*	This Paper	N/A
Arabidopsis thaliana: *pAGO10D1*	This Paper	N/A
Arabidopsis thaliana: *pAGO1::YFP-AGO1*	This Paper	N/A
Arabidopsis thaliana: *p35S:: AGO10*	Yu et al., 2017	N/A
Arabidopsis thaliana: *pSTM::STM-Venus*	Heisler et al., 2005	N/A
Arabidopsis thaliana: *pREV::REV-Venus*	Heisler et al., 2005	N/A
Arabidopsis thaliana: *p35S::STM-GR*	Heisler et al., 2005	N/A
Arabidopsis thaliana: *pDR5::GFP*	Heisler et al., 2005	N/A
Arabidopsis thaliana: *p35S::DII-Venus*	Vernoux et al., 2011	N/A
Arabidopsis thaliana: *pnh-2*	Arabidopsis Biological Resource Center	CS3853
Arabidopsis thaliana: *ago10–13*	Ji et al., 2011	N/A
Oligonucleotides		
Primers		Table S1
Recombinant DNA		
pAGO10::GFPer	This Paper	N/A

REAGENT or RESOURCE	SOURCE	IDENTIFIER
pAGO10Δ1::GFPer	This Paper	N/A
pAGO10Δ34:GFPer	This Paper	N/A
pAGO1::YFP-AGO1	This Paper	N/A
pAGO10::LUC	This Paper	N/A
pYAO:CAS9- pAGO10	This Paper	N/A
pAGO10Δ1::LUC	This Paper	N/A
pAGO10Δ2::LUC	This Paper	N/A
pAGO10Δ12::LUC	This Paper	N/A
pAGO10Δ3::LUC	This Paper	N/A
pAGO10Δ4::LUC	This Paper	N/A
p35S::BZR1-GFP	This Paper	N/A
p35S::ARF5-GFP	This Paper	N/A
p35S::PIF4-GFP	This Paper	N/A
Software and Algorithms		
Image J	NIH	https://imagej.nih.gov/ij/